ELSEVIER

Comput. Methods Appl. Mech. Engrg. 188 (2000) 567–594

Computer methods in applied mechanics and engineering

www.elsevier.com/locate/cma

A co-rotational finite element formulation for buckling and postbuckling analyses of spatial beams

Kuo Mo Hsiao *, Wen Yi Lin

Department of Mechanical Engineering, National Chiao Tung University, 1001 TA Hsueh Road, Hsinchu, Taiwan, ROC

Received 2 September 1998

Abstract

A consistent co-rotational finite element formulation and numerical procedure for the buckling and postbuckling analyses of three-dimensional elastic Euler beam is presented. All coupling among bending, twisting, and stretching deformations for a beam element is considered by consistent second-order linearization of the fully geometrically nonlinear beam theory. However, the third-order terms, which are relevant to the twist rate and curvature of the beam axis, are also considered. An incremental–iterative method based on the Newton–Raphson method combined with constant arc length of incremental displacement vector is employed for the solution of nonlinear equilibrium equations. The zero value of the tangent stiffness matrix determinant of the structure is used as the criterion of the buckling state. A bisection method of the arc length is proposed to find the buckling load. Numerical examples are presented to demonstrate the accuracy and efficiency of the proposed method and to investigate the effect of third-order terms on the buckling load and postbuckling behavior of three-dimensional beams.

1. Introduction

The buckling and postbuckling analyses of spatial beams have been the subject of considerable research [1–24]. The buckling of the beam structures is caused by the coupling among bending, twisting, and stretching deformations of the beam members. Thus the buckling analysis is a subtopic of nonlinear rather than linear mechanics [8]. The linear buckling analysis of the beam has been extensively studied, and many valuable results have been reported in the literature [1–17]. In [17] a consistent co-rotational finite element formulation and numerical procedure for the linear buckling analysis of three-dimensional elastic Euler beam is presented. A limitation of finite element formulation for the linear buckling analysis of beam problems has been the omission of any consideration of the effect of prebuckling deflections of the beam. This omission may be sufficiently accurate when the prebuckling deflection of the beam is negligible. In other cases, however, the effect of the prebuckling deflections must be taken into account if the buckling load is to be determined with accuracy [8,17]. Moreover, the linear buckling analysis gives no information about the shape of the secondary path. Sometimes the behavior of a structure can be understood only if the shape of the secondary shape is known. Thus, many different formulations and numerical procedures for the buckling and postbuckling analyses of the three-dimensional beam have been proposed [1–8,18–24]. Currently, the most popular approach for the analysis of the three-dimensional beam is to develop finite element models. The formulations, which have been used in the literature, might be divided into three

* Corresponding author. Fax: +886-35-720-634.
E-mail address: kmhsiao@cc.nctu.edu.tw (K.M. Hsiao).

0045-7825/00/$ - see front matter
PII: S0045-7825(99)00284-4

categories: total Lagrangian (TL) formulation [14,18,22,23,25,26], updated Lagrangian (UL) formulation [23,25], and co-rotational (CR) formulation [17,19,27]. It is well known that within the co-rotating system either a TL or a UL formulation may be employed [27,28]. These formulations are consequently termed CR–TL and CR–UL formulations. The reference configuration used in a CR–TL formulation differs from the one used in a conventional TL formulation by the motion performed by the co-rotating coordinate system from the initial to the current (or neighboring) configuration. In order to capture correctly all coupling among bending, twisting, and stretching deformations of the beam elements, the formulation of beam elements might be derived by the fully geometrically nonlinear beam theory [29]. The exact expressions for the element nodal forces, which are required in a TL formulation for large displacement/small strain problems, are highly nonlinear functions of element nodal parameters. However, the dominant factors in the geometrical nonlinearities of beam structures are attributable to finite rotations, the strains remaining small. For a beam structure discretized by finite elements, this implies that the motion of the individual elements to a large extent will consist of rigid body motion. If the rigid body motion part is eliminated from the total displacements and the element size is properly chosen, the deformational part of the motion is always small relative to the local element axes; thus in conjunction with the co-rotational formulation, the higher-order terms of nodal parameters in the element nodal forces may be neglected by consistent linearization [27,29]. The so-called 'Natural approach' by Argyris and co-workers, for instance [1–7], is also based on the idea of separating rigid body motions from local deformations. It has been used in various applications such as linear, large displacement/small strain, and large strain problems. The co-rotational formulation has been extensively applied in the nonlinear analysis. However, to the authors' knowledge, the application of co-rotational formulation in the nonlinear buckling and postbuckling analyses has not been reported in the literature. The object of this paper is to investigate the effect of prebuckling deflections on the buckling load of beam structures and to investigate the postbuckling behavior of beam structures using the co-rotational total Lagrangian formulation.

In [27], Hsiao presented a co-rotational total Lagrangian formulation of the beam element for the nonlinear analysis of three-dimensional beam structures with large rotations but small strains. Element deformations and element equations are defined in terms of element coordinates which are constructed at the current configuration of the beam element. The element deformations are determined by the rotation of element cross-section coordinates, which are rigidly tied to element cross section, relative to the element coordinate system. In order to capture correctly all coupling among bending, twisting, and stretching deformations of the beam elements, the formulation of the beam element is derived by consistent second-order linearization of the fully geometrically nonlinear beam theory. This element is proven to be very effective for geometrically nonlinear analysis of the three-dimensional beams by numerical examples studied in [27]. However, the third-order terms of the nodal parameters are not considered in [27]. It is reported in [30] that the third-order term of twist rate of the beam axis is not negligible for the geometrically nonlinear analysis of the cantilever beam with narrow rectangular cross section under twist. The values of twist rate and curvature of the beam axis are deformation dependent, not element size dependent. Thus their values may not always be much smaller than unity. It seems that some third-order terms, which are relevant to the twist rate and curvature of the beam axis, may not be negligible for some cross sections with large rotations. Here, the formulation of the beam element proposed in [30] is employed, and the third-order terms of nodal parameters, which are relevant to the twist rate and curvature of the beam axis, are also considered.

An incremental–iterative method based on the Newton–Raphson method combined with constant arc length of incremental displacement vector is employed for the solution of nonlinear equilibrium equations. The zero value of the tangent stiffness matrix determinant of the structure is used as the criterion of the buckling state, and the corresponding load is the so-called buckling load. A bisection method of the arc length is proposed to find the buckling load. An inverse power method for the solution of the generalized eigenvalue problem is used to find the corresponding buckling mode. In order to initiate the secondary path, at the bifurcation point a perturbation displacement proportional to the first buckling mode is added [31]. Numerical examples are presented to demonstrate the accuracy and efficiency of the proposed method and to investigate the effect of third-order terms on the buckling load and postbuckling behavior of three-dimensional beams.

2. Finite element formulation

In the following only a brief description of the beam element is given. The more detailed description may be obtained from [27].

2.1. Basic assumptions

The following assumptions are made in derivation of the beam element behavior:

1. The beam is prismatic and slender, and the Euler–Bernoulli hypothesis is valid.
2. The cross section of the beam is doubly symmetric.
3. The unit extension and the twist rate of the centroid axis of the beam element are uniform.
4. The cross section of the beam element does not deform in its own plane and strains within this cross section can be neglected.
5. The out-of-plane warping of the cross section is the product of the twist rate of the beam element and the Saint Venant warping function for a prismatic beam of the same cross section.
6. The deformation displacements of the beam element are small.

2.2. Coordinate systems

In this paper, a co-rotational total Lagrangian formulation is adopted. In order to describe the system, we define four sets of right-handed rectangular Cartesian coordinate systems:

1. A fixed global set of coordinates, X_i^G $(i = 1, 2, 3)$ (see Fig. 1): the nodal coordinates, displacements, and rotations, and the stiffness matrix of the system are defined in these coordinates.

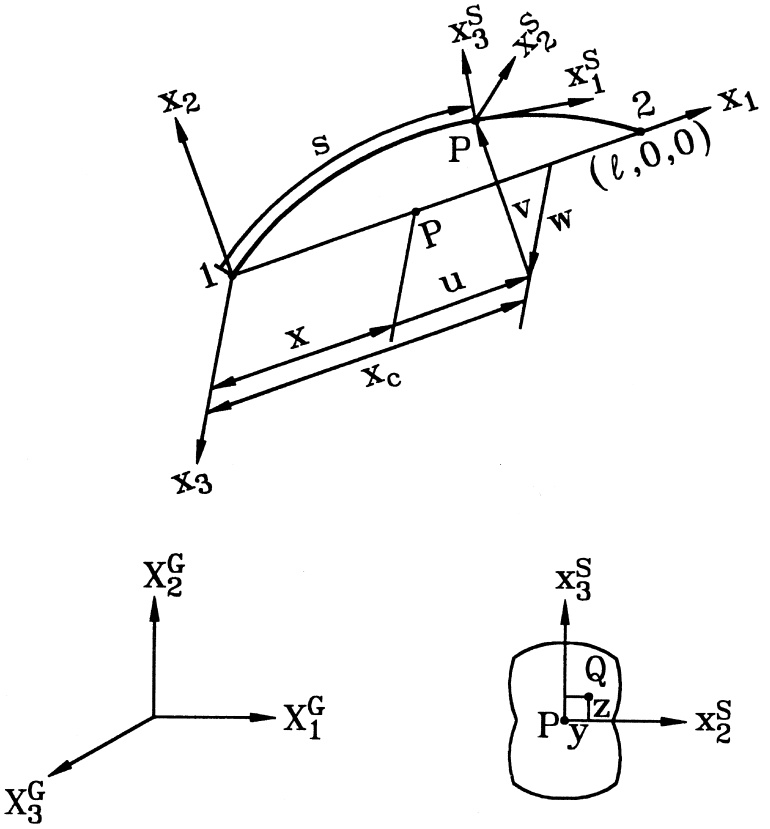

Fig. 1. Coordinate systems.

2. Element cross-section coordinates, x_i^S $(i = 1, 2, 3)$ (see Fig. 1): a set of element cross-section coordinates is associated with each cross section of the beam element. The origin of this coordinate system is rigidly tied to the centroid of the cross section. The x_1^S axes are chosen to coincide with the normal of the unwrapped cross section and the x_2^S and x_3^S axes are chosen to be the principal directions of the cross section.

3. Element coordinates, x_i $(i = 1, 2, 3)$ (see Fig. 1): a set of element coordinates is associated with each element, which is constructed at the current configuration of the beam element. The origin of this coordinate system is located at node 1, and the x_1 axis is chosen to pass through two end nodes of the element; the x_2 and x_3 axes are chosen to be the principal directions of the cross section at the undeformed state. *Note that this coordinate system is a local coordinate system not a moving coordinate system.* The deformations, internal nodal forces and stiffness matrix of the elements are defined in terms of these coordinates. In this paper the element deformations are determined by the rotation of element cross-section coordinate systems relative to this coordinate system.

4. Load base coordinates, X_i^P $(i = 1, 2, 3)$: a set of load base coordinates is associated with each configuration-dependent moment. The origin of this coordinate system is chosen to be the node where the configuration-dependent moment is applied. The mechanism for generating configuration-dependent moment is described in these coordinates, and the corresponding external load and load stiffness matrix are defined in terms of these coordinates.

In this paper, the symbol { } denotes the column matrix. The relations among the global coordinates, element cross-section coordinates, element coordinates and load base coordinates may be expressed by

$$\mathbf{X}^G = \mathbf{A}_{GS}\mathbf{x}^S, \qquad \mathbf{X}^G = \mathbf{A}_{GE}\mathbf{x}, \qquad \mathbf{X}^G = \mathbf{A}_{GP}\mathbf{X}^P, \tag{1}$$

where $\mathbf{X}^G = \{X_1^G, X_2^G, X_3^G\}$, $\mathbf{x}^S = \{x_1^S, x_2^S, x_3^S\}$, $\mathbf{x} = \{x_1, x_2, x_3\}$, and $\mathbf{X}^P = \{X_1^P, X_2^P, X_3^P\}$; $\mathbf{A}_{GS}$, $\mathbf{A}_{GE}$, and $\mathbf{A}_{GP}$ are matrices of direction cosines of the surface coordinate system, element coordinate system, and load base coordinate system, respectively.

2.3. Rotation vector and rotation parameters

For the convenience of later discussion, the term 'rotation vector' is used to represent a finite rotation. Fig. 2 shows a vector $\mathbf{b}$ which as a result of the application of a rotation vector $\phi\mathbf{a}$ is transported to the new position $\bar{\mathbf{b}}$. The relation between $\bar{\mathbf{b}}$ and $\mathbf{b}$ may be expressed as [32]

$$\bar{\mathbf{b}} = \cos\phi\mathbf{b} + (1 - \cos\phi)(\mathbf{a}\cdot\mathbf{b})\mathbf{a} + \sin\phi(\mathbf{a}\times\mathbf{b}), \tag{2}$$

where ϕ is the angle of counterclockwise rotation, and $\mathbf{a}$ is the unit vector along the axis of rotation.

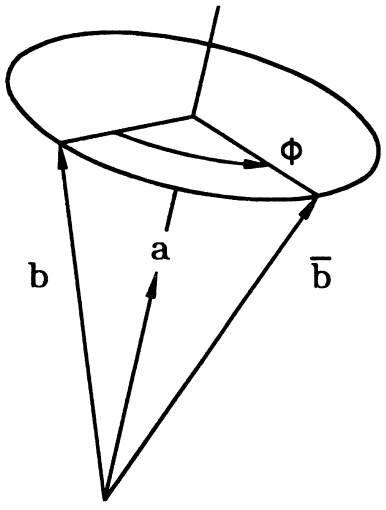

Fig. 2. Rotation vector.

Let $\mathbf{e}_i$ and $\mathbf{e}_i^S$ $(i = 1, 2, 3)$ denote the unit vectors associated with the x_i and x_i^S axes, respectively. Here, the traid $\mathbf{e}_i^S$ in the deformed state is assumed to be achieved by the successive application of the following two rotation vectors to the traid $\mathbf{e}_i$:

$$\boldsymbol{\theta}_n = \theta_n \mathbf{n} \tag{3}$$

and

$$\boldsymbol{\theta}_t = \theta_1 \mathbf{t}, \tag{4}$$

where

$$\mathbf{n} = \left\{0, \theta_2 \Big/ (\theta_2^2 + \theta_3^2)^{1/2}, \theta_3 \Big/ (\theta_2^2 + \theta_3^2)^{1/2}\right\} = \{0,\ n_2,\ n_3\}, \tag{5}$$

$$\mathbf{t} = \{\cos\theta_n,\ \theta_3, -\theta_2\}, \tag{6}$$

$$\cos\theta_n = (1 - \theta_2^2 - \theta_3^2)^{1/2}, \tag{7}$$

$$\theta_2 = -\frac{\mathrm{d}w(s)}{\mathrm{d}s}, \qquad \theta_3 = \frac{\mathrm{d}v(s)}{\mathrm{d}s} \tag{8}$$

in which $\mathbf{n}$ is the unit vector perpendicular to the vectors $\mathbf{e}_1$ and $\mathbf{e}_1^S$, and $\mathbf{t}$ is the tangent unit vector of the deformed centroid axis of the beam element. Note that $\mathbf{e}_1^S$ coincides with $\mathbf{t}$. θ_1 is the rotation about vector $\mathbf{t}$. θ_n is the inverse of $\cos\theta_n$. $v(s)$ and $w(s)$ are the lateral deflections of the centroid axis of the beam element in the x_2 and x_3 directions, respectively, and s is the arc length of the deformed centroid axis.

Using Eqs. (2)–(8), the relation between the vectors $\mathbf{e}_i$ and $\mathbf{e}_i^S$ $(i = 1, 2, 3)$ in the element coordinate system may be obtained as

$$\mathbf{e}_i^S = [\mathbf{t}, \mathbf{R}_1, \mathbf{R}_2]\mathbf{e}_i = \mathbf{R}\mathbf{e}_i, \tag{9}$$

$$\begin{aligned}
&\mathbf{R}_1 = \cos\theta_1 \mathbf{r}_1 + \sin\theta_1 \mathbf{r}_2, \qquad \mathbf{R}_2 = -\sin\theta_1 \mathbf{r}_1 + \cos\theta_1 \mathbf{r}_2,\\
&\mathbf{r}_1 = \left\{-\theta_3, \cos\theta_n + (1 - \cos\theta_n)n_2^2, (1 - \cos\theta_n)n_2 n_3\right\},\\
&\mathbf{r}_2 = \left\{\theta_2, (1 - \cos\theta_n)n_2 n_3, \cos\theta_n + (1 - \cos\theta_n)n_3^2\right\},
\end{aligned} \tag{10}$$

where $\mathbf{R}$ is the so-called rotation matrix. The rotation matrix is determined by θ_i $(i = 1, 2, 3)$. Thus, θ_i are called rotation parameters in this study.

Let $\boldsymbol{\theta} = \{\theta_1, \theta_2, \theta_3\}$ be the column matrix of rotation parameters, $\delta\boldsymbol{\theta}$ be the variation of θ. The traid $\mathbf{e}_i^S$ $(i = 1, 2, 3)$ corresponding to $\boldsymbol{\theta}$ may be rotated by a rotation vector $\delta\boldsymbol{\phi} = \{\delta\phi_1, \delta\phi_1, \delta\phi_1\}$ to reach their new positions corresponding to $\boldsymbol{\theta} + \delta\boldsymbol{\theta}$ [27]. When θ_2 and θ_3 are much smaller than unity, the relationship between $\delta\boldsymbol{\theta}$ and $\delta\boldsymbol{\phi}$ may be approximated by [27]

$$\delta\boldsymbol{\theta} = \begin{bmatrix} 1 & \theta_3/2 & -\theta_2/2 \\ -\theta_3 & 1 & 0 \\ \theta_2 & 0 & 1 \end{bmatrix} \delta\boldsymbol{\phi} = \mathbf{T}^{-1}\delta\boldsymbol{\phi}. \tag{11}$$

2.4. Nodal parameters and forces

The element employed here has two nodes with six degrees of freedom per node. Two sets of element nodal parameters termed 'explicit nodal parameters' and 'implicit nodal parameters' are employed. The

explicit nodal parameters of the element are used for the assembly of the system equations from the element equations. They are chosen to be u_{ij}, the x_i $(i = 1, 2, 3)$ components of the translation vectors $\mathbf{u}_j$ at node j $(j = 1, 2)$ and ϕ_{ij}, the x_i $(i = 1, 2, 3)$ components of the rotation vectors $\boldsymbol{\phi}_j$ at node j $(j = 1, 2)$. Here, the values of $\boldsymbol{\phi}_j$ are reset to zero at current configuration. Thus, $\delta\phi_{ij}$, the variation of ϕ_{ij}, represents infinitesimal rotations about the x_i axes [27], and the generalized nodal forces corresponding to $\delta\phi_{ij}$ are m_{ij}, the conventional moments about the x_i axes. The generalized nodal forces corresponding to δu_{ij}, the variations of u_{ij}, are f_{ij}, the forces in the x_i directions.

The implicit nodal parameters of the element are used to determine the deformation of the beam element. They are chosen to be u_{ij}, the x_i $(i = 1, 2, 3)$ components of the translation vectors $\mathbf{u}_j$ at node j $(j = 1, 2)$ and θ_{ij}, the nodal values of the rotation parameters θ_i $(i = 1, 2, 3)$ at node j $(j = 1, 2)$. The generalized nodal forces corresponding to δu_{ij} and $\delta\theta_{ij}$ are f_{ij} and m^{θ}_{ij}, the forces in the x_i directions and the generalized moments, respectively. Note that m^{θ}_{ij} are not conventional moments, because $\delta\theta_{ij}$ are not infinitesimal rotations about the x_i axes at deformed state.

In view of Eq. (11), the relations between the variation of the implicit and explicit nodal parameters may be expressed as

$$\delta\mathbf{q}_{\theta} = \begin{Bmatrix} \delta\mathbf{u}_1 \\ \delta\boldsymbol{\theta}_1 \\ \delta\mathbf{u}_2 \\ \delta\boldsymbol{\theta}_2 \end{Bmatrix} = \begin{bmatrix} \mathbf{I} & \mathbf{0} & \mathbf{0} & \mathbf{0} \\ \mathbf{0} & \mathbf{T}_1^{-1} & \mathbf{0} & \mathbf{0} \\ \mathbf{0} & \mathbf{0} & \mathbf{I} & \mathbf{0} \\ \mathbf{0} & \mathbf{0} & \mathbf{0} & \mathbf{T}_2^{-1} \end{bmatrix} \begin{Bmatrix} \delta\mathbf{u}_1 \\ \delta\boldsymbol{\phi}_1 \\ \delta\mathbf{u}_2 \\ \delta\boldsymbol{\phi}_2 \end{Bmatrix} = \mathbf{T}_{\theta\phi}\delta\mathbf{q}, \tag{12}$$

where $\delta\mathbf{u}_j = \{\delta u_{1j}, \delta u_{2j}, \delta u_{3j}\}$, $\delta\boldsymbol{\theta}_j = \{\delta\theta_{1j}, \delta\theta_{2j}, \delta\theta_{3j}\}$ and $\delta\boldsymbol{\phi}_j = \{\delta\phi_{1j}, \delta\phi_{2j}, \delta\phi_{3j}\}$ $(j = 1, 2)$; $\mathbf{I}$ and $\mathbf{0}$ are the identity and zero matrices of order 3×3, respectively; $\mathbf{T}_j^{-1}$ $(j = 1, 2)$ are nodal values of $\mathbf{T}^{-1}$ given in Eq. (11).

Let $\mathbf{f} = \{\mathbf{f}_1, \mathbf{m}_1, \mathbf{f}_2, \mathbf{m}_2\}$, $\mathbf{f}_{\theta} = \{\mathbf{f}_1, \mathbf{m}^{\theta}_1, \mathbf{f}_2, \mathbf{m}^{\theta}_2\}$, where $\mathbf{f}_j = \{f_{1j}, f_{2j}, f_{3j}\}$, $\mathbf{m}_j = \{m_{1j}, m_{2j}, m_{3j}\}$, and $\mathbf{m}^{\theta}_j = \{m^{\theta}_{1j}, m^{\theta}_{2j}, m^{\theta}_{3j}\}$ $(j = 1, 2)$, denote the internal nodal force vectors corresponding to the variation of the explicit and implicit nodal parameters, $\delta\mathbf{q}$ and $\delta\mathbf{q}_{\theta}$, respectively. Using the contragradient law [33] and Eq. (12), the relation between $\mathbf{f}$ and $\mathbf{f}_{\theta}$, may be given by

$$\mathbf{f} = \mathbf{T}^{\mathrm{t}}_{\theta\phi}\mathbf{f}_{\theta}. \tag{13}$$

The global nodal parameters for the system of equations corresponding to the element local nodes j $(j = 1, 2)$ should be consistent with the element explicit nodal parameters. Thus, they are chosen to be U_{ij}, the X_i $(i = 1, 2, 3)$ components of the translation vectors $\mathbf{U}_j$ at node j $(j = 1, 2)$ and Φ_{ij}, the X_i $(i = 1, 2, 3)$ components of the rotation vectors $\boldsymbol{\Phi}_j$ at nodes j $(j = 1, 2)$. Here, the values of $\boldsymbol{\Phi}_j$ are reset to zero at current configuration. Thus, $\delta\Phi_{ij}$, the variations of Φ_{ij}, represent infinitesimal rotations about the X_i axes [27], and the generalized nodal forces corresponding to $\delta\Phi_{ij}$ are the conventional moments about the X_i axes. The generalized nodal forces corresponding to δU_{ij}, the variation of U_{ij}, are the forces in the X_i directions.

2.5. Kinematics of beam element

The deformations of the beam element are described in the current element coordinate system. From the kinematic assumptions made in this paper, the deformations of the beam element may be determined by the displacements of the centroid axis of the beam element, orientation of the cross section (element cross-section coordinates), and the out-of-plane warping of the cross section. Let Q (Fig. 1) be an arbitrary point in the beam element, and P be the point corresponding to Q on the centroid axis. The position vector of point Q in the undeformed and deformed configurations may be expressed as

$$\mathbf{r}_0 = x\mathbf{e}_1 + y\mathbf{e}_2 + z\mathbf{e}_3 \tag{14}$$

and

$$\mathbf{r} = x_c(s)\mathbf{e}_1 + v(s)\mathbf{e}_2 + w(s)\mathbf{e}_3 + \theta_{1,s}\omega(y, z)\mathbf{e}^s_1 + y\mathbf{e}^s_2 + z\mathbf{e}^s_3, \tag{15}$$

where $x_c(s)$, $v(s)$, and $w(s)$ are the x_1, x_2 and x_3 coordinates of point P, respectively, s is the arc length of the deformed centroid axis measured from node 1 to point P, and $\omega(y,z)$ is the Saint Venant warping function. The relationship among $x_c(s)$, $v(s)$, $w(s)$, and s may be given as

$$x_c(s) = u_{11} + \int_0^s \cos\theta_n \, \mathrm{d}s, \tag{16}$$

where u_{11} is the displacement of node 1 in the x_1 direction, and $\cos\theta_n$ is defined in Eq. (7). Note that due to the definition of the element coordinate system, the value of u_{11} is equal to zero. However, the variation of u_{11} is not zero. Making use of Eq. (16), one obtains

$$S = \frac{2l}{\int_{-1}^{1} \cos\theta_n \, \mathrm{d}\xi}, \tag{17}$$

$$l = x_c(S) - x_c(0) = L - u_{11} + u_{12} \tag{18}$$

and

$$\xi = -1 + \frac{2s}{S} \tag{19}$$

in which S and l are the current arc length and chord length of the centroid axis of the beam element, respectively, and L is the chord length of the undeformed beam axis.

Here, the lateral deflections of the centroid axis $v(s)$ and $w(s)$ are assumed to be the Hermitian polynomials of s, and the rotation about the centroid axis $\theta_1(s)$ (Eq. (4)) is assumed to be linear polynomials of s. $v(s)$, $w(s)$, and $\theta_1(s)$ may be expressed by

$$\begin{aligned} v(s) &= \{N_1, N_2, N_3, N_4\}^{\mathrm{t}} \{u_{21}, \theta_{31}, u_{22}, \theta_{32}\} = \mathbf{N}_b^{\mathrm{t}} \mathbf{u}_b, \\ w(s) &= \{N_1, -N_2, N_3, -N_4\}^{\mathrm{t}} \{u_{31}, \theta_{21}, u_{32}, \theta_{22}\} = \mathbf{N}_c^{\mathrm{t}} \mathbf{u}_c, \\ \theta_1(s) &= \{N_5, N_6\}^{\mathrm{t}} \{\theta_{11}, \theta_{12}\} = \mathbf{N}_d^{\mathrm{t}} \mathbf{u}_d, \end{aligned} \tag{20}$$

where u_{2j} and u_{3j} $(j = 1,2)$ are nodal values of v and w at nodes j, respectively, and θ_{ij} $(i = 1,2,3,\ j = 1,2)$ are nodal values of θ_i at nodes j. Note that, due to the definition of the element coordinates, the values of u_{2j} and u_{3j} $(j = 1,2)$ are zero. However, their variations are not zero. N_i $(i = 1,\ldots,6)$ are shape functions and are given by

$$\begin{aligned} &N_1 = \frac{1}{4}(1-\xi)^2(2+\xi), \quad N_2 = \frac{1}{8}S(1-\xi^2)(1-\xi), \quad N_3 = \frac{1}{4}(1+\xi)^2(2-\xi), \\ &N_4 = \frac{1}{8}S(-1+\xi^2)(1+\xi), \quad N_5 = \frac{1}{2}(1-\xi), \quad N_6 = \frac{1}{2}(1+\xi). \end{aligned} \tag{21}$$

The axial displacements of the centroid axis may be determined from the lateral deflections and the unit extension of the centroid axis using Eq. (16).

If x, y and z in Eq. (14) are regarded as the Lagrangian coordinates, the Green strain ε_{11}, ε_{12} and ε_{13} are given by [34]

$$\varepsilon_{11} = \frac{1}{2}(\mathbf{r}_{,x}^{\mathrm{t}} \mathbf{r}_{,x} - 1), \quad \varepsilon_{12} = \frac{1}{2}\mathbf{r}_{,x}^{\mathrm{t}} \mathbf{r}_{,y}, \quad \varepsilon_{13} = \frac{1}{2}\mathbf{r}_{,x}^{\mathrm{t}} \mathbf{r}_{,z}. \tag{22}$$

Using the chain rule for differentiation, $\mathbf{r}_{,x}$ in Eq. (22) may be expressed as

$$\mathbf{r}_{,x} = \mathbf{r}_{,s}(1+\varepsilon_0), \tag{23}$$

$$\varepsilon_0 = \frac{\partial s}{\partial x} - 1, \tag{24}$$

where ε_0 is the unit extension of the centroid axis. Making use of the assumption of uniform unit extension, one may rewrite Eq. (24) as

$$\varepsilon_0 = \frac{S}{L} - 1. \tag{25}$$

Substituting Eqs. (5)–(10), (15), (23) and (25) into Eq. (22) and retaining terms up to the second-order of nodal parameters yield

$$\begin{aligned}
\varepsilon_{11} &= \varepsilon_0 + \frac{1}{2}\varepsilon_0^2 + (1+\varepsilon_0)^2\left[y(-\theta_{3,s}+\theta_{2,s}\theta_1) + z(\theta_{2,s}+\theta_{3,s}\theta_1) + \frac{1}{2}y^2(\theta_{1,s}^2+\theta_{3,s}^2)\right.\\
&\quad \left. + \frac{1}{2}z^2(\theta_{1,s}^2+\theta_{2,s}^2) - yz\theta_{2,s}\theta_{3,s}\right],\\
\varepsilon_{12} &= \frac{1}{2}(1+\varepsilon_0)\left[(-z+\omega_{,y})\theta_{1,s} + \frac{1}{2}z(\theta_2\theta_{3,s}-\theta_3\theta_{2,s}) + \omega_{,y}\theta_{1,s}(z\theta_{2,s}-y\theta_{3,s}) + \theta_{1,s}\theta_{3,s}\omega\right],\\
\varepsilon_{13} &= \frac{1}{2}(1+\varepsilon_0)\left[(y+\omega_{,z})\theta_{1,s} + \frac{1}{2}y(\theta_3\theta_{2,s}-\theta_2\theta_{3,s}) + \omega_{,z}\theta_{1,s}(z\theta_{2,s}-y\theta_{3,s}) - \theta_{1,s}\theta_{2,s}\omega\right],
\end{aligned} \tag{26}$$

$$\varepsilon_0 = \frac{l}{L}\left[1 + \frac{1}{4}\int_{-1}^{1}(\theta_2^2+\theta_3^2)\,\mathrm{d}\xi\right] - 1. \tag{27}$$

2.6. Element nodal force vector

The element nodal force vector $\mathbf{f}_\theta$ (Eq. (13)) corresponding to the implicit nodal parameters is obtained from the virtual work principle in the current element coordinates. It should be mentioned again that *the element coordinate system is a local coordinate system not a moving coordinate system.* Thus, a standard procedure is used here for the derivation of $\mathbf{f}_\theta$. For convenience, the implicit nodal parameters are divided into four generalized nodal displacement vectors $\mathbf{u}_i$ $(i = a, b, c, d)$, where

$$\mathbf{u}_a = \{u_{11}, u_{12}\} \tag{28}$$

and $\mathbf{u}_b$, $\mathbf{u}_c$, and $\mathbf{u}_d$ are defined in Eq. (20).

The generalized force vectors corresponding to $\delta\mathbf{u}_i$, the variation of $\mathbf{u}_i$ $(i = a, b, c, d)$ are

$$\mathbf{f}_a = \{f_{11}, f_{12}\}, \quad \mathbf{f}_b = \{f_{21}, m_{31}^\theta, f_{22}, m_{32}^\theta\}, \quad \mathbf{f}_c = \{f_{31}, m_{21}^\theta, f_{32}, m_{22}^\theta\}, \quad \mathbf{f}_d = \{m_{11}^\theta, m_{12}^\theta\}. \tag{29}$$

The virtual work principle requires that

$$\delta\mathbf{u}_a^{\mathrm{t}}\mathbf{f}_a + \delta\mathbf{u}_b^{\mathrm{t}}\mathbf{f}_b + \delta\mathbf{u}_c^{\mathrm{t}}\mathbf{f}_c + \delta\mathbf{u}_d^{\mathrm{t}}\mathbf{f}_d = \int_V (\sigma_{11}\delta\varepsilon_{11} + 2\sigma_{12}\delta\varepsilon_{12} + 2\sigma_{13}\delta\varepsilon_{13})\,\mathrm{d}V, \tag{30}$$

where V is the volume of the undeformed beam, $\delta\varepsilon_{1j}$ $(j = 1, 2, 3)$ are the variation of ε_{1j} in Eq. (26), respectively, with respect to the implicit nodal parameter. σ_{1j} $(j = 1, 2, 3)$ are the second Piola–Kirchhoff stress. For linear elastic material, the following constitutive equations are used:

$$\sigma_{11} = E\varepsilon_{11}, \qquad \sigma_{12} = 2G\varepsilon_{12}, \quad \text{and} \quad \sigma_{13} = 2G\varepsilon_{13} \tag{31}$$

in which E is Young's modulus and G is shear modulus.

If the element size is chosen small enough, the values of the rotation parameters of the deformed element defined in the current element coordinate system may always be much smaller than unity. Thus the

higher-order terms of rotation parameters in the element internal nodal forces may be neglected. However, in order to include the nonlinear coupling among the bending, twisting, and stretching deformations, the terms up to the second-order of rotation parameters and their spatial derivatives are retained in element internal nodal forces by consistent second-order linearization of Eq. (30). The values of spatial derivatives of the rotation parameters, which are relevant to the twist rate and curvature of the beam axis, are deformation dependent, not element size dependent. Thus their values may not always be much smaller than unity and their third-order terms may not be negligible. Here, the third-order terms of the spatial derivatives of the rotation parameters are also retained in Eq. (30). From Eqs. (26)–(31), we may obtain

$$\mathbf{f}_a = AEL\varepsilon_0\left(1+\frac{3}{2}\varepsilon_0\right)\mathbf{G}_a + \left[EI_y\int\left(\frac{5}{2}\theta_{2,s}^2-\theta_{2,s}\theta_{2,s}^*\right)\mathrm{d}s + EI_z\int\left(\frac{5}{2}\theta_{3,s}^2-\theta_{3,s}\theta_{3,s}^*\right)\mathrm{d}s + \frac{1}{2}EI_p\int\theta_{1,s}^2\,\mathrm{d}s\right]\mathbf{G}_a, \tag{32}$$

$$\mathbf{f}_b = EI_z(1+4\varepsilon_0)\int\mathbf{N}_b''\theta_{3,s}\,\mathrm{d}s + f_{12}\mathbf{G}_b - E(I_z-I_y)\int\mathbf{N}_b''\theta_1\theta_{2,s}\,\mathrm{d}s + \frac{1}{2}GJ\int\left(\mathbf{N}_b'\theta_{1,s}\theta_{2,s}-\mathbf{N}_b''\theta_{1,s}\theta_2\right)\mathrm{d}s + \underline{\frac{1}{2}EK_z\int\mathbf{N}_b''\theta_{3,s}^3\,\mathrm{d}s + \frac{1}{2}E(K_z+K_{yz})\int\mathbf{N}_b''\theta_{1,s}^2\theta_{3,s}\,\mathrm{d}s + \frac{3}{2}EK_{yz}\int\mathbf{N}_b''\theta_{2,s}^2\theta_{3,s}\,\mathrm{d}s}, \tag{33}$$

$$\mathbf{f}_c = -EI_y(1+\varepsilon_0)\int\mathbf{N}_c''\theta_{2,s}\,\mathrm{d}s + f_{12}\mathbf{G}_c + E\left(I_z-I_y\right)\int\mathbf{N}_c''\theta_1\theta_{3,s}\,\mathrm{d}s + \frac{1}{2}GJ\int\left(\mathbf{N}_c'\theta_{1,s}\theta_{3,s}-\mathbf{N}_c''\theta_{1,s}\theta_3\right)\mathrm{d}s - \underline{\frac{1}{2}EK_y\int\mathbf{N}_c''\theta_{2,s}^3\,\mathrm{d}s - \frac{1}{2}E(K_y-K_{yz})\int\mathbf{N}_c''\theta_{1,s}^2\theta_{2,s}\,\mathrm{d}s - \frac{3}{2}EK_{yz}\int\mathbf{N}_c''\theta_{3,s}^2\theta_{2,s}\,\mathrm{d}s}, \tag{34}$$

$$\mathbf{f}_d = GJ(1+\varepsilon_0)\int\mathbf{N}_d'\theta_{1,s}\,\mathrm{d}s + EI_p\varepsilon_0\int\mathbf{N}_d'\theta_{1,s}\,\mathrm{d}s - \frac{1}{2}GJ\int\mathbf{N}_d'(\theta_2\theta_{3,s}-\theta_3\theta_{2,s})\,\mathrm{d}s - E(I_z-I_y)\int\mathbf{N}_d\theta_{2,s}\theta_{3,s}\,\mathrm{d}s + \underline{\frac{1}{2}EK_I\int\mathbf{N}_d'\theta_{1,s}^3\,\mathrm{d}s + \frac{1}{2}E(K_y+K_{yz})\int\mathbf{N}_d'\theta_{2,s}^2\theta_{1,s}\,\mathrm{d}s + \frac{1}{2}E(K_z+K_{yz})\int\mathbf{N}_d'\theta_{3,s}^2\theta_{1,s}\,\mathrm{d}s}, \tag{35}$$

where

$$\begin{aligned}
&\mathbf{G}_a = \frac{1}{L}\{-1,1\},\quad \mathbf{G}_b = \int\mathbf{N}_b'\theta_3\,\mathrm{d}s,\quad \mathbf{G}_c = -\int\mathbf{N}_c'\theta_2\,\mathrm{d}s,\quad \theta_{3,s}^* = \{2N_1'',N_2'',2N_3'',N_4''\}^{\mathrm{t}}\mathbf{u}_b = \mathbf{N}_b^{*''\mathrm{t}}\mathbf{u}_b,\\
&\theta_{2,s}^* = -\{2N_1'',-N_2'',2N_3'',-N_4''\}^{\mathrm{t}}\mathbf{u}_c = -\mathbf{N}_c^{*''\mathrm{t}}\mathbf{u}_c,\quad I_y = \int z^2\,\mathrm{d}A,\quad I_z = \int y^2\,\mathrm{d}A,\quad I_p = I_y+I_z,\\
&K_y = \int z^4\,\mathrm{d}A,\quad K_{yz} = \int y^2z^2\,\mathrm{d}A,\quad K_z = \int y^4\,\mathrm{d}A,\quad K_I = K_y+K_z+2K_{yz},\\
&J = \int\left[(-z+\omega_{,y})^2+(y+\omega_{,z})^2\right]\mathrm{d}A
\end{aligned} \tag{36}$$

in which the range of integration for the integral $\int(\,)\,\mathrm{d}s$ in Eqs. (32)–(36) is from 0 to S, A is the cross-section area, $\mathbf{N}_j$ $(j=b,c,d)$ are given in Eq. (21), $(\,)' = \mathrm{d}(\,)/\mathrm{d}s$. The underlined terms in Eqs. (32)–(35) are the third-order terms of the spatial derivatives of the rotation parameters.

The element nodal force vector $\mathbf{f}$ (Eq. (13)) corresponding to the explicit nodal parameters may be obtained from Eqs. (13) and (32)–(35). Note that only the terms up to the second-order of nodal parameters and the third-order terms of the spatial derivatives of the rotation parameters are retained in $\mathbf{f}$.

2.7. Element tangent stiffness matrices

The element tangent stiffness matrix corresponding to the explicit nodal parameters (referred to as explicit tangent stiffness matrix) may be obtained by differentiating the element nodal force vector $\mathbf{f}$ in Eq. (13) with respect to explicit nodal parameters. Using Eqs. (12) and (13), we obtain

$$\mathbf{k} = \frac{\partial \mathbf{f}}{\partial \mathbf{q}} = \frac{\partial \mathbf{f}}{\partial \mathbf{q}_\theta}\frac{\partial \mathbf{q}_\theta}{\partial \mathbf{q}} = \mathbf{T}_{\theta\phi}^{\mathrm{T}}\mathbf{k}_\theta\mathbf{T}_{\theta\phi} + \mathbf{H}, \tag{37}$$

where $\mathbf{k}_\theta = \partial \mathbf{f}_\theta/\partial \mathbf{q}_\theta$ is the tangent stiffness matrix corresponding to implicit nodal parameters (referred to as implicit tangent stiffness matrix), and $\mathbf{H}$ is an unsymmetrical matrix and is given by

$$\mathbf{H} = \begin{bmatrix} \mathbf{0} & \mathbf{0} & \mathbf{0} & \mathbf{0} \\ \mathbf{0} & \mathbf{H}_1 & \mathbf{0} & \mathbf{0} \\ \mathbf{0} & \mathbf{0} & \mathbf{0} & \mathbf{0} \\ \mathbf{0} & \mathbf{0} & \mathbf{0} & \mathbf{H}_2 \end{bmatrix} \tag{38}$$

in which $\mathbf{0}$ is a zero matrix of order 3×3 and

$$\mathbf{H}_j = \begin{bmatrix} 0 & m_{3j}^\theta & -m_{2j}^\theta \\ 0 & 0 & \frac{1}{2}m_{1j}^\theta \\ 0 & -\frac{1}{2}m_{1j}^\theta & 0 \end{bmatrix}. \tag{39}$$

Using the direct stiffness method, the implicit tangent stiffness matrix $\mathbf{k}_\theta$ may be assembled by the submatrices

$$\mathbf{k}_{ij} = \frac{\partial \mathbf{f}_i}{\partial \mathbf{u}_j}, \tag{40}$$

where $\mathbf{f}_i$ $(i = a, b, c, d)$ are defined in Eqs. (32)–(35) and $\mathbf{u}_i$ $(i = a, b, c, d)$ are defined in Eqs. (20) and (28). The explicit form of $\mathbf{k}_{ij}$ may be expressed as

$$\mathbf{k}_{aa} = AEL(1+3\varepsilon_0)\mathbf{G}_a\mathbf{G}_a^{\mathrm{t}},$$

$$\mathbf{k}_{ab} = \mathbf{k}_{ba}^{\mathrm{t}} = AE\mathbf{G}_a\mathbf{G}_b^{\mathrm{t}} + EI_z\mathbf{G}_a\left[\int \mathbf{N}_b''^{\mathrm{t}}(5\theta_{3,s} - \theta_{3,s}^*)\,\mathrm{d}s - \int \mathbf{N}_b^{*\prime\prime\mathrm{t}}\theta_{3,s}\,\mathrm{d}s\right],$$

$$\mathbf{k}_{ac} = \mathbf{k}_{ca}^{\mathrm{t}} = AE\mathbf{G}_a\mathbf{G}_c^{\mathrm{t}} + EI_y\left[\mathbf{G}_a\int \mathbf{N}_c''^{\mathrm{t}}(5\theta_{2,s} - \theta_{2,s}^*)\,\mathrm{d}s - \int \mathbf{N}_c^{*\prime\prime\mathrm{t}}\theta_{2,s}\,\mathrm{d}s\right],$$

$$\mathbf{k}_{ad} = \mathbf{k}_{da}^{\mathrm{t}} = EI_p\mathbf{G}_a\int \mathbf{N}_d'^{\mathrm{t}}\theta_{1,s}\,\mathrm{d}s,$$

$$\mathbf{k}_{bb} = EI_z(1+4\varepsilon_0)\int \mathbf{N}_b''\mathbf{N}_b''^{\mathrm{t}}\,\mathrm{d}s + f_{12}\int \mathbf{N}_b'\mathbf{N}_b'^{\mathrm{t}}\,\mathrm{d}s + \underline{\frac{1}{2}E(K_z+K_{yz})\int \mathbf{N}_b''\mathbf{N}_b''^{\mathrm{t}}\theta_{1,s}^2\,\mathrm{d}s}$$
$$\underline{+\frac{3}{2}EK_{yz}\int \mathbf{N}_b''\mathbf{N}_b''^{\mathrm{t}}\theta_{2,s}^2\,\mathrm{d}s + \frac{3}{2}EK_z\int \mathbf{N}_b''\mathbf{N}_b''^{\mathrm{t}}\theta_{3,s}^2\,\mathrm{d}s},$$

$$\mathbf{k}_{bc} = \mathbf{K}_{cb}^{\mathrm{t}}$$
$$= E(I_z - I_y)\int \mathbf{N}_b''\mathbf{N}_c''^{\mathrm{t}}\theta_1\,\mathrm{d}s + \frac{1}{2}GJ\int (\mathbf{N}'\prime_b\mathbf{N}_c''^{\mathrm{t}} - \mathbf{N}_b'\mathbf{N}_c''^{\mathrm{t}})\theta_{1,s}\,\mathrm{d}s, \underline{-3EK_{yz}\int \mathbf{N}_b''\mathbf{N}_c''^{\mathrm{t}}\theta_{2,s}\theta_{3,s}\,\mathrm{d}s},$$

$$\mathbf{k}_{bd} = \mathbf{k}_{db}^{\mathrm{t}} = -E\left(I_z - I_y\right)\int \mathbf{N}_b''\mathbf{N}_d'^{\mathrm{t}}\theta_{2,s}\,\mathrm{d}s - \frac{1}{2}GJ\int \mathbf{N}_b''\mathbf{N}_d'^{\mathrm{t}}\theta_2\,\mathrm{d}s + \frac{1}{2}GJ\int \mathbf{N}_b'\mathbf{N}_d'^{\mathrm{t}}\theta_{2,s}\,\mathrm{d}s$$
$$\underline{+E(K_z+K_{yz})\int \mathbf{N}_b''\mathbf{N}_d'^{\mathrm{t}}\theta_{1,s}\theta_{3,s}\,\mathrm{d}s},$$

$$
\begin{aligned}
\mathbf{k}_{cc} &= EI_y(1+4\varepsilon_0)\int \mathbf{N}_c''\mathbf{N}_c''^{\mathrm{t}}\,\mathrm{d}s + f_{12}\int \mathbf{N}_c'\mathbf{N}_c'^{\mathrm{t}}\,\mathrm{d}s \\
&\quad + \underline{\frac{1}{2}E(K_y+K_{yz})\int \mathbf{N}_c''\mathbf{N}_c''^{\mathrm{t}}\theta_{1,s}^2\,\mathrm{d}s + \frac{3}{2}EK_y\int \mathbf{N}_c''\mathbf{N}_c''^{\mathrm{t}}\theta_{2,s}^2\,\mathrm{d}s + \frac{3}{2}EK_{yz}\int \mathbf{N}_c''\mathbf{N}_c''^{\mathrm{t}}\theta_{3,s}^2\,\mathrm{d}s}, \\
\mathbf{k}_{cd} &= \mathbf{k}_{dc}^{\mathrm{t}} = E(I_z-I_y)\int \mathbf{N}_c''\mathbf{N}_d'^{\mathrm{t}}\theta_{3,s}\,\mathrm{d}s - \frac{1}{2}GJ\int \mathbf{N}_c''\mathbf{N}_d'^{\mathrm{t}}\theta_3\,\mathrm{d}s + \frac{1}{2}GJ\int \mathbf{N}_c'\mathbf{N}_d'^{\mathrm{t}}\theta_{3,s}\,\mathrm{d}s \\
&\quad \underline{- E(K_y+K_{yz})\int \mathbf{N}_c''\mathbf{N}_d'^{\mathrm{t}}\theta_{1,s}\theta_{2,s}\,\mathrm{d}s}, \\
\mathbf{k}_{dd} &= GJ(1+2\varepsilon_0)\int \mathbf{N}_d'\mathbf{N}_d'^{\mathrm{t}}\,\mathrm{d}s + EI_p\varepsilon_0\int \mathbf{N}_d'\mathbf{N}_d'^{\mathrm{t}}\,\mathrm{d}s + \underline{\frac{3}{2}EK_I\int \mathbf{N}_d'\mathbf{N}_d'^{\mathrm{t}}\theta_{1,s}^2\,\mathrm{d}s} \\
&\quad + \underline{\frac{1}{2}E(K_y+K_{yz})\int \mathbf{N}_d'\mathbf{N}_d'^{\mathrm{t}}\theta_{2,s}^2\,\mathrm{d}s + \frac{1}{2}E(K_z+K_{yz})\int \mathbf{N}_d'\mathbf{N}_d'^{\mathrm{t}}\theta_{3,s}^2\,\mathrm{d}s},
\end{aligned}
\tag{41}
$$

where the underlined terms are the second-order terms of the spatial derivatives of the rotation parameters.

Note that because only the terms up to the second-order of nodal parameters and the third-order terms of the spatial derivatives of the rotation parameters are retained in **f**, only the terms up to the first-order of nodal parameters and the second-order terms of the spatial derivatives of the rotation parameters are retained in the element stiffness matrix given in Eq. (37). The element tangent stiffness matrix referred to the global coordinate system is obtained by using the standard coordinate transformation.

2.8. Load stiffness matrix

Different ways for generating configuration-dependent moment were proposed in the literature [3,4,13,17]. Here, for simplicity, only the conservative moments generated by conservative force or forces (with fixed directions) are considered, and the ways for generating conservative moment proposed in [17] are employed here. For completeness, a brief description of the ways for generating conservative moment is given here. In this study, a set of load base coordinates X_i^P $(i=1,2,3)$ associated with each configuration-dependent moment are constructed at the current configuration. The mechanism for generating configuration-dependent moment is described in these coordinates, and the corresponding external load and load stiffness matrix [35] are defined in terms of these coordinates. Unless stated otherwise, all vectors and matrices in this section are referred to these coordinates. Note that this coordinate system is just a local coordinate system constructed at the current configuration, not a moving coordinate system. Thus, it is regarded as a fixed coordinated system in the derivation of the load stiffness matrix.

The first way of generating configuration-dependent moment may be described as follows.

Consider a sphere of radius R whose centroid is rigidly connected with the structure at node O as shown in Fig. 3. Two strings wound around a great circle of the sphere are acted upon by forces of magnitude P**.** Thus, the strings are always tangent to the sphere. The great circle and the forces are on the same plane at the undeformed configuration of the structure. However, the great circle and the forces are generally not on the same plane when the structure is deformed. The origin of the load base coordinate system is chosen to be located at the node O. The X_1^P axis is chosen to coincide with the normal of the plane of the great circle, and the X_2^P and X_3^P axes lie in the plane of the great circle.

Let A denote the contact point of the force **P** and the great circle. Because **P** is tangent to the sphere, **P** is perpendicular to the line OA. Let $\mathbf{e}_A$ denote unit vector in the direction of line OA. $\mathbf{e}_A$ may be expressed by

$$
\mathbf{e}_A = \mathbf{a}/(\mathbf{a}^{\mathrm{t}}\mathbf{a})^{1/2}, \tag{42}
$$

$$
\mathbf{a} = \mathbf{e}_p^P \times \mathbf{n}^P = \{0, l_3, -l_2\}, \tag{43}
$$

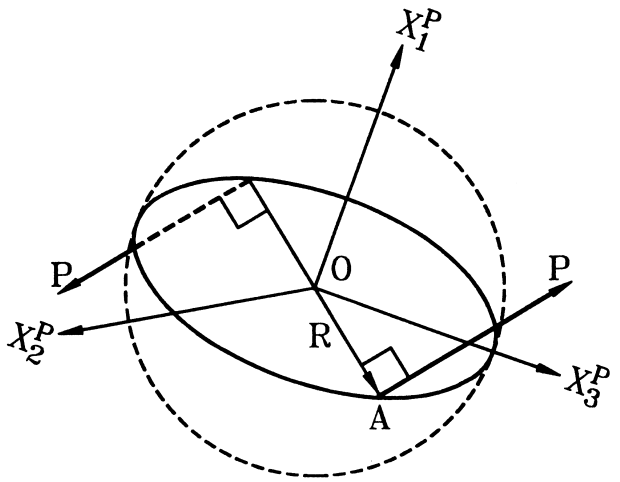

Fig. 3. Mechanism for generating configuration dependent moment.

where $\mathbf{e}_p^P = \{l_1, l_2, l_3\}$ is the unit vector in the direction of $\mathbf{P}$, and $\mathbf{n}^P$ is the unit normal of the plane of the great circle. Note that $\mathbf{n}^P$ coincides with $\mathbf{e}_1^P = \{1, 0, 0\}$, the unit vector associated with the X_1^P axis.

The external moment vector at node O generated by the above-mentioned mechanism may be expressed by

$$\mathbf{M} = M\,\mathbf{e}_A \times \mathbf{e}_p^P, \tag{44}$$

where $M = 2RP$ is the magnitude of the moment. The corresponding load stiffness matrix $\mathbf{k}_p$ may be expressed as

$$\mathbf{k}_p = M(l_2^2 + l_3^2)^{-1/2}\mathbf{k}_{pa} + M(l_2^2 + l_3^2)^{-3/2}\mathbf{k}_{pb}, \tag{45}$$

where

$$\mathbf{k}_{pa} = \begin{bmatrix} 0 & l_1 l_3 & -l_1 l_2 \\ 0 & l_2 l_3 & l_1^2 + l_3^2 \\ 0 & -l_1^2 - l_2^2 & -l_2 l_3 \end{bmatrix}, \tag{46}$$

$$\mathbf{k}_{pb} = \begin{bmatrix} 0 & -l_1 l_3(l_2^2 + l_3^2) & l_1 l_2(l_2^2 + l_3^2) \\ 0 & l_1^2 l_2 l_3 & -l_1^2 l_2^2 \\ 0 & l_1^2 l_3^2 & -l_1^2 l_2 l_3 \end{bmatrix}. \tag{47}$$

Three special cases shown in Fig. 4 are considered here. Following [3,4], they are referred to as quasi-tangential (QT) moments of the first and second type, and semitangential (ST) moment. The load stiffness matrices corresponding to QT and ST moments at the configurations shown in Fig. 4 may be obtained from Eqs. (45)–(47) and given by

$$\mathbf{k}_p^{\mathrm{QT1}} = M \begin{bmatrix} 0 & 0 & 0 \\ 0 & 0 & 0 \\ 0 & -1 & 0 \end{bmatrix}, \tag{48}$$

$$\mathbf{k}_p^{\mathrm{QT2}} = M \begin{bmatrix} 0 & 0 & 0 \\ 0 & 0 & 1 \\ 0 & 0 & 0 \end{bmatrix}, \tag{49}$$

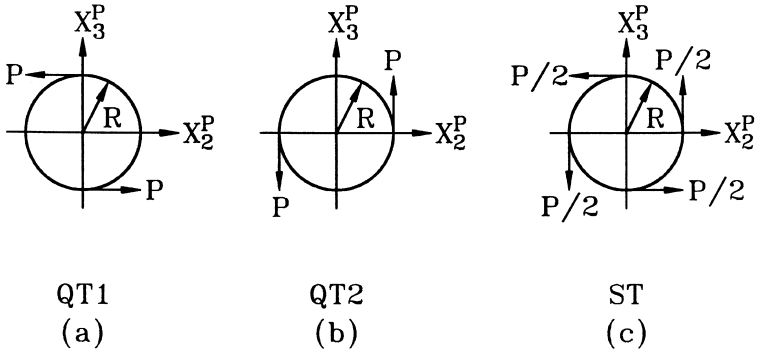

Fig. 4. Quasitangential (QT) moment and semitangential (ST) moment.

$$\mathbf{k}_p^{\mathrm{ST}} = \frac{M}{2}\begin{bmatrix} 0 & 0 & 0 \\ 0 & 0 & 1 \\ 0 & -1 & 0 \end{bmatrix}. \tag{50}$$

The second way for generating configuration-dependent moment may described as follows.

Consider a rigid arm of length R whose end is rigidly connected with the structure at node O as shown in Fig. 5. The other end of the rigid arm is acted upon by a conservative force (with a fixed direction) of magnitude P. The origin of the load base coordinates X_i^P $(i = 1, 2, 3)$ is chosen to be located at the node O. The X_1^P axis is chosen to coincide with the axis of the rigid arm, and the X_2^P and X_3^P axes are perpendicular to the rigid arm.

The external moment vector at node O generated by the above-mentioned mechanism may be expressed by

$$\mathbf{M} = RP\mathbf{t}^P \times \mathbf{e}_p^P, \tag{51}$$

where $\mathbf{e}_p^P = \{l_1, l_2, l_3\}$is the unit vector in the direction of $\mathbf{P}$, and $\mathbf{t}^P$ is the unit vector in the axial direction of the rigid arm. Note that $\mathbf{t}^P$ coincides with $\mathbf{e}_1^P = \{1, 0, 0\}$, the unit vector associated with the X_1^P axis. The corresponding load stiffness matrix may be expressed as

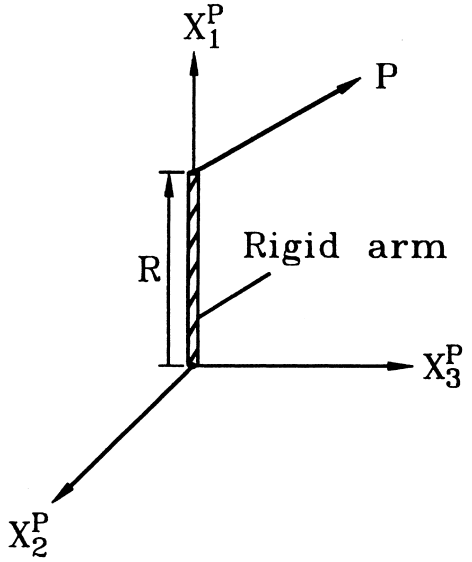

Fig. 5. Mechanism for generating configuration dependent moment by an off-axis load.

$$\mathbf{k}_p = RP \begin{bmatrix} 0 & l_2 & l_3 \\ 0 & -l_1 & 0 \\ 0 & 0 & -l_1 \end{bmatrix}. \tag{52}$$

The load stiffness matrix referred to the global coordinate system is obtained by using the standard coordinate transformation and may be expressed by

$$\mathbf{k}_p^G = \mathbf{A}_{GP}\mathbf{k}_p\mathbf{A}_{GP}^{\mathrm{t}}, \tag{53}$$

where $\mathbf{A}_{GP}$ is the transformation matrix given in Eq. (1).

2.9. Equilibrium equations

The nonlinear equations of motion may be expressed by

$$\Psi = \mathbf{F} - \lambda\mathbf{P} = \mathbf{0}, \tag{54}$$

where Ψ is the unbalanced force between the internal nodal force $\mathbf{F}$ and the external nodal force $\lambda\mathbf{P}$, where λ is the loading parameter, and $\mathbf{P}$ is a reference loading. Note that $\mathbf{P}$ may require to be updated at each iteration if the applied load is configuration dependent. $\mathbf{F}$ is assembled from the element nodal force vectors, which are calculated using Eqs. (13) and (32)–(35) first in the current element coordinates and then transformed from current element coordinate system to global coordinate system before assemblage using the standard procedure.

In this paper, a weighted Euclidean norm of the unbalanced force is employed for the equilibrium iterations, and is given by

$$\frac{\|\Psi\|}{\sqrt{N}} \leqslant e_{\mathrm{tol}}, \tag{55}$$

where N is the number of equations of the system, and e_{tol} is a prescribed value of error tolerance.

2.10. Criterion of the buckling state

Here, the zero value of the tangent stiffness matrix determinant is used as the criterion of the buckling state. The tangent stiffness matrix of the structure is assembled from the element stiffness matrix and load stiffness matrix. Let $\mathbf{K}_{\mathrm{T}}(\lambda)$ denote the tangent stiffness matrix of the structure corresponding to the loading parameter λ. The criterion of the buckling state may be expressed as

$$D(\lambda) = \det|\mathbf{K}_{\mathrm{T}}(\lambda)| = 0. \tag{56}$$

Let λ_{NB} denote the minimum root of Eq. (56). λ_{NB} is the loading parameter corresponding to buckling state. The buckling mode corresponding to λ_{NB} may be obtained by solving the following generalized eigenvalue problem

$$\mathbf{K}_0\mathbf{X} = -\frac{\lambda}{\lambda_{\mathrm{NB}}}\mathbf{K}_G\mathbf{X}, \tag{57}$$

where $\mathbf{K}_0$ is the linear stiffness matrix of the structure, and $\mathbf{K}_{\mathrm{G}} = \mathbf{K}_{\mathrm{T}} - \mathbf{K}_0$ is the geometric stiffness matrix of the structure corresponding to λ_{NB}. The eigenvector corresponding to eigenvalue λ_{NB} is the required buckling mode. Here, the inverse power method [36] is used to find the buckling load and buckling mode.

3. Numerical algorithm

An incremental–iterative method based on the Newton–Raphson method combined with constant arc length of incremental displacement vector [37,38] is employed for the solution of nonlinear equilibrium equations. For a given displacement increment or corrector, the method described in [27,39] is employed to determine the current element cross-section coordinates, element coordinates and element deformation nodal parameters for each element. A bisection method of the arc length is proposed here to find the buckling load. In order to initiate the secondary path, at the bifurcation point a perturbation displacement proportional to the first buckling mode is added [31].

The basic steps involved in the bisection method are outlined as follows.

Assume that the equilibrium configuration of the Ith incremental step is obtained. Let ΔS_I denote the arc length of the incremental displacement vector of the Ith incremental step, and λ_I and $\mathbf{K}_{\mathrm{T}}^I$ denote loading parameter and tangent stiffness matrix corresponding to the equilibrium configuration of the Ith incremental step, respectively. If $\mathbf{K}_{\mathrm{T}}^{I-1}$ is positive definite and $\mathbf{K}_{\mathrm{T}}^I$ is positive nondefinite, the following steps are used to obtain the buckling load:

1. Let $\Delta S_{\mathrm{L}} = 0,\ \Delta S_{\mathrm{R}} = \Delta S_I,\ \lambda_{\mathrm{L}} = 0,$ and $\lambda_{\mathrm{R}} = \lambda_I$.
2. Let $\Delta S_I = (\Delta S_{\mathrm{L}} + \Delta S_{\mathrm{R}})/2$. Repeat the Ith incremental step to obtain a new λ_I and $\mathbf{K}_{\mathrm{T}}^I$.
3. If $\mathbf{K}_{\mathrm{T}}^I$ is positive definite, let $\Delta S_{\mathrm{L}} = \Delta S_I$, and $\lambda_{\mathrm{L}} = \lambda_I$. If $\mathbf{K}_{\mathrm{T}}^I$ is positive nondefinite, let $\Delta S_{\mathrm{R}} = \Delta S_I$, and $\lambda_{\mathrm{R}} = \lambda_I$.
4. Let $\lambda_I = (\lambda_{\mathrm{L}} + \lambda_{\mathrm{R}})/2$. If $|\lambda_{\mathrm{L}} - \lambda_{\mathrm{R}}|/\lambda_I \leqslant E_\lambda$, where E_λ is a prescribed error tolerance, stop the iteration; otherwise go to step 2.

The buckling load λ_{NB} is chosen to be the converged λ_I.

4. Numerical studies

In order to investigate the effect of third-order terms on the buckling load and postbuckling behavior of three-dimensional beams, the following cases are considered:

1. NF = 1 – All the terms up to the second-order in Eqs. (32)–(35), and the corresponding terms in Eq. (41) are considered.

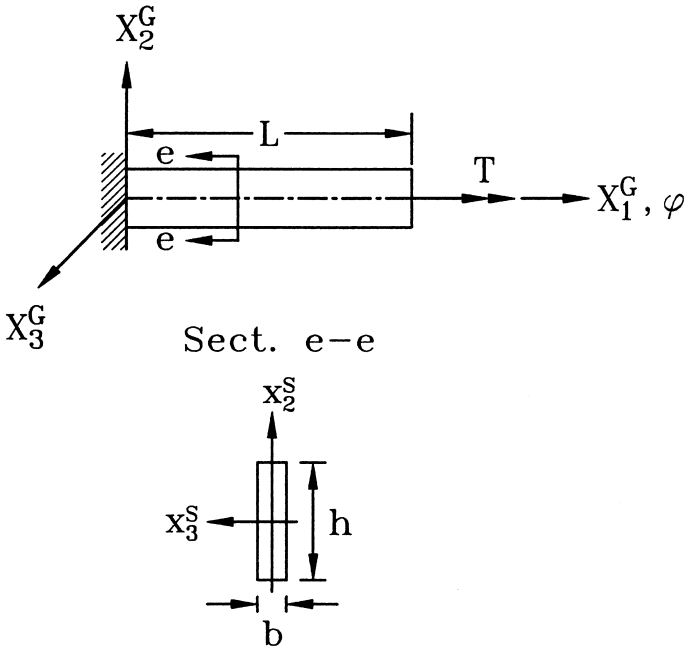

Fig. 6. Cantilever beam subjected to end torsion.

2. NF = 2 – Except the term $EI_p\varepsilon_0 \int \mathbf{N}'_d\theta_{1,s}\,ds$ in Eq. (35), all the terms up to the second-order in Eqs. (32)–(35), and the corresponding terms in Eq. (41) are considered.
3. NF = 3 – The third-order term $(1/2)EK_I \int N'_d\theta^3_{1,s}\,ds$ in Eq. (35) and all the terms up to the second-order in Eqs. (32)–(35), and the corresponding terms in Eq. (41) are considered.
4. NF = 4 – All the terms in Eqs. (32)–(35), and Eq. (41) are considered.

4.1. Example 1. Cantilever beam subjected to end torsion

The example considered here is a cantilever beam subjected to end torsion T as shown in Fig. 6. Because only the primary path is considered for this example, the ways of generating end moment are rendered irrelevant here. The geometry and material properties of the beam are: $b = 0.5$ cm, $h = 10$ cm, $L = 100$ cm, cross-sectional area $A = 5$ cm^2, moment of inertia about x^S_2 axis $I_y = 0.1042$ cm^4, moment of inertia about x^S_3 axis $I_z = 41.67$ cm^4, torsional constant $J = 0.4167$ cm^4, $K_I = 626.6$ cm^6, Young's modulus $E = 2.1 \times 10^6$ kP/cm^2, and shear modulus $G = 7.875 \times 10^5$ kP/cm^2.

It is observed that the only nonzero deformations are uniform twist rate $\theta_{1,s}$ and uniform unit extension of the centroid axis ε_0 for this example. From Eq. (32), and using the approximation $1 + (3/2)\varepsilon_0 \approx 1$, one may obtain

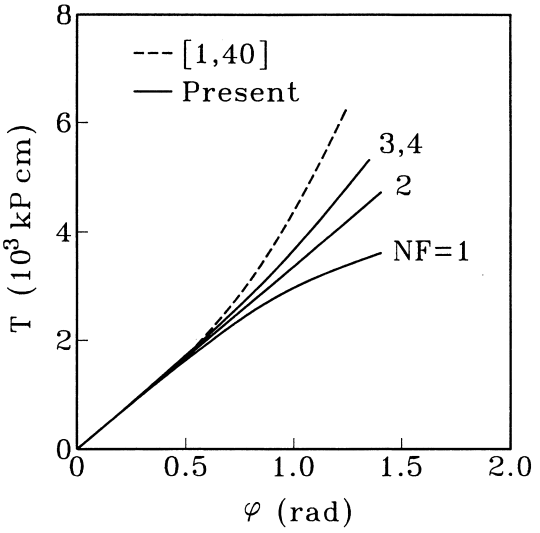

Fig. 7. Load–end twist angle for cantilever beam subjected to end torsion.

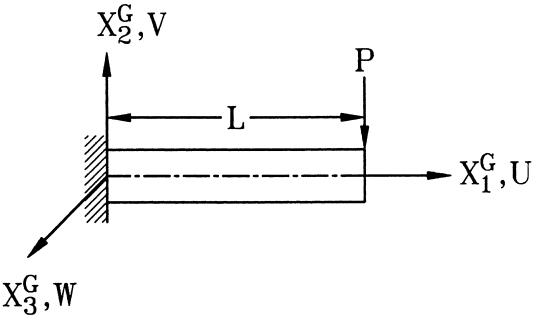

Fig. 8. Cantilever beam subjected to end force.

$$\varepsilon_0 = -\frac{I_p}{2A}\theta_{1,s}^2. \tag{58}$$

As can be seen from Eq. (58) ε_0 is a second-order term of twist rate. Thus $EI_p\varepsilon_0 \int \mathbf{N}_a'\theta_{1,s}\,\mathrm{d}s$ in Eq. (35) may be regarded as a third-order term of $\theta_{1,s}$. From Eq. (35), and using the approximation $1 + (1/2)\varepsilon_0 \approx 1$, one may obtain the constitutive equation for twist moment for different cases as follows:

$$T = m_1^\theta = GJ\theta_{1,s} - \frac{EI_p^2}{2A}\theta_{1,s}^3 \quad \text{for NF} = 1, \tag{59}$$

$$T = m_1^\theta = GJ\theta_{1,s} \quad \text{for NF} = 2 \tag{60}$$

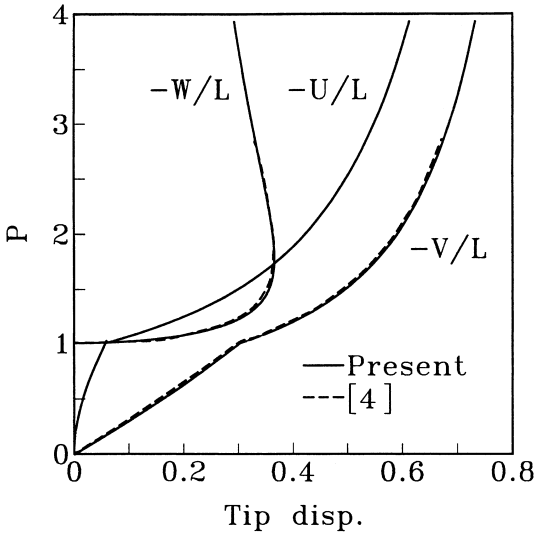

Fig. 9. Load–tip displacements for cantilever beam subjected to end force.

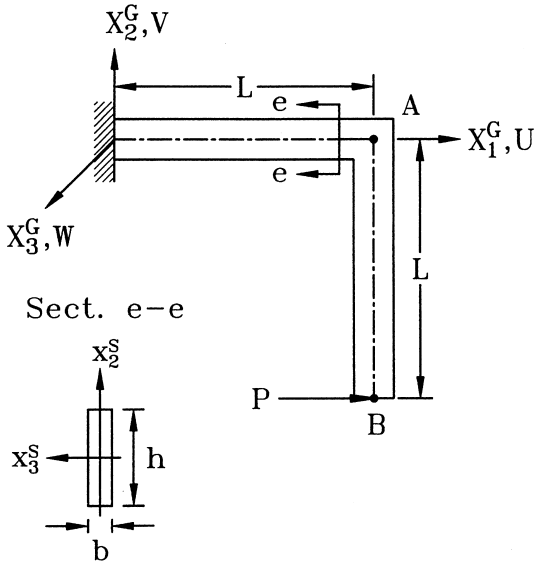

Fig. 10. Cantilever angle subjected to a horizontal end force.

and

$$T = m_1^{\theta} = GJ\theta_{1,s} + \frac{1}{2}E\left(K_I - \frac{EI_p^2}{A}\right)\theta_{1,s}^3 \quad \text{for NF} = 3,4. \tag{61}$$

It is seen that linear twist moment–twist rate relation is used for NF = 2, and nonlinear twist moment–twist rate relations are used for NF = 1, 3, 4. However, the third-order term for NF = 1 is incomplete.

The present results obtained by using 20 elements are shown in Fig. 7 together with the results of [1,2,40]. The results of [1,2,40] are obtained using triangular facet shell element. The agreement among all results is very good when twist rate is small. The results of NF = 1, may be unreasonable when the twist rate is not small, because the torsional rigidity decreases with the increase of the twist angle. The agreement between the results of NF = 3, 4 and the results given in [1,2,40] is qualitatively good, each set showing increase of torsional rigidity with the increase of twist angle. Quantitatively there are considerable differences. These may be attributed at least in part to that the theory of the shell is two-dimensional and the theory of beam is one-dimensional. However, the results of NF = 3, 4 are more reliable than the results of NF = 1 and 2. Thus NF = 3, or 4 may be required for reasonable solutions.

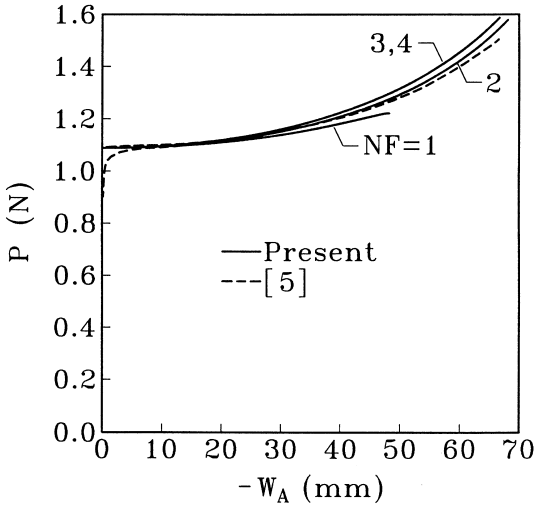

Fig. 11. Load–displacement for cantilever angle subjected to end force.

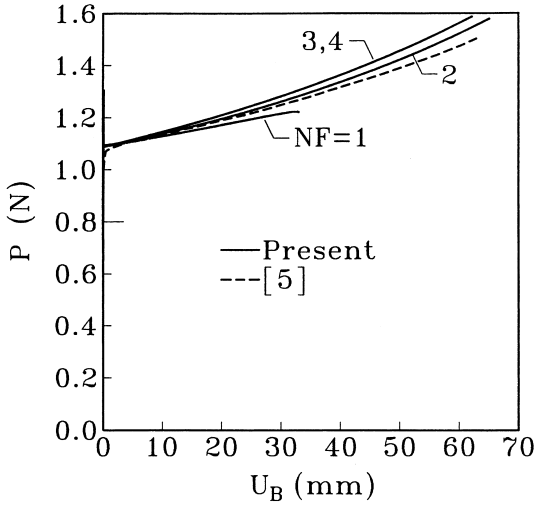

Fig. 12. Load–displacement for cantilever angle subjected to end force.

4.2. Example 2. Cantilever beam subjected to end force

This example was first introduced by Argyris et al. [3,4]. The example considered is a cantilever beam subjected to a lateral end force P as shown in Fig. 8. The X_i^G $(i = 1, 2, 3)$ axes of the global coordinate system shown in Fig. 8 coincide with x_i^S axes, the axes of the element cross-section coordinate system in the undeformed beam. The geometry and material properties are: length $L = 100$, cross-sectional area $A = 1.0$, moment of inertia about x_2^S axis $I_y = 0.125$, moment of inertia about x_3^S axis $I_z = 1.0$, torsional constant $J = 0.5$, Young's modulus $E = 10^4$, and shear modulus $G = 5 \times 10^3$. The classical buckling load for this example is $P_{cr} = (4.013/L^2)\sqrt{EI_yGJ} = 0.7094$ [11].

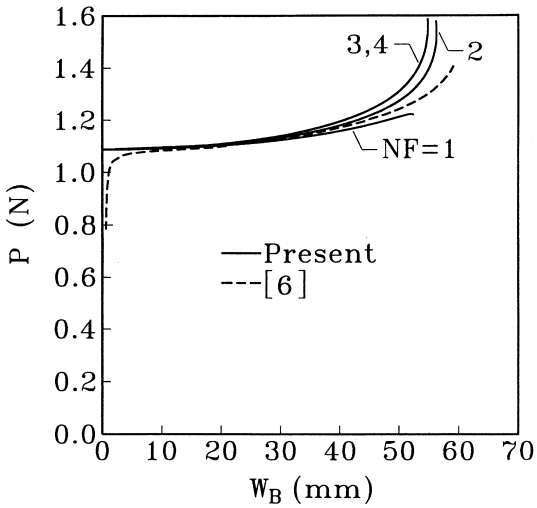

Fig. 13. Load–displacement for cantilever angle subjected to end force.

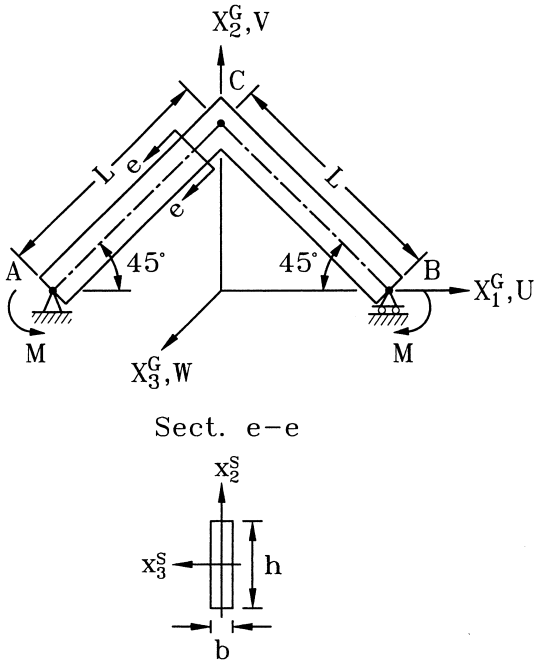

Fig. 14. Simply supported angle subjected to uniform moment.

Twenty elements are used for discretization. Because the cross-section constants K_y, K_z, and K_{yz} (see Eq. (36)) are not given in [3,4], only the cases NF = 1, 2 are considered. The results for these two cases are nearly identical. Thus, only the results for the case NF = 2 are reported. The nonlinear buckling load obtained here is $P_{NB} = 1.0069$. The load–deflection curves of the present study together with the results of [3,4] are shown in Fig. 9. Very good agreement among all these solutions is observed. Because the pre-buckling displacements for this example are quite large, the discrepancy between the nonlinear buckling load and classical linear buckling load is remarked.

4.3. Example 3. Cantilever angle subjected to a horizontal end force

The example considered here is a cantilever angle subjected to a horizontal force P at the centroid of the end cross section as shown in Fig. 10. The geometry and material properties are: $L = 240$ mm, $b = 0.6$ mm, $h = 30$ mm, cross-sectional area $A = 18$ mm^2, moment of inertia about x_2^S axis $I_y = 0.54$ mm^4, moment of inertia about x_3^S axis $I_z = 1350$ mm^4, torsional constant $J = 2.16$ mm^4, $K_I = 1.823 \times 10^5$ mm^6, Young's modulus $E = 71240$ N/mm^2, and shear modulus $G = 27190$ N/mm^2.

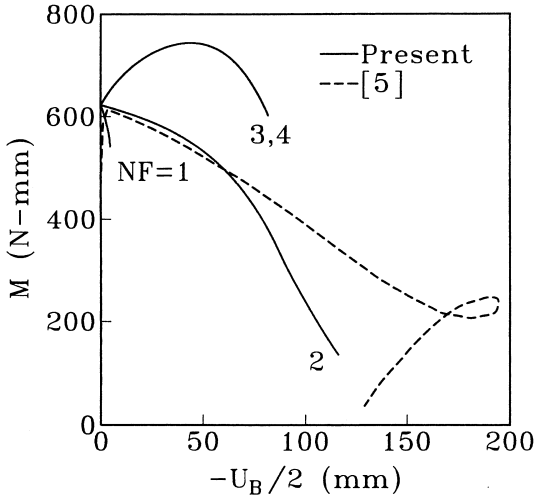

Fig. 15. Load–displacement for simply supported angle subjected to uniform moment.

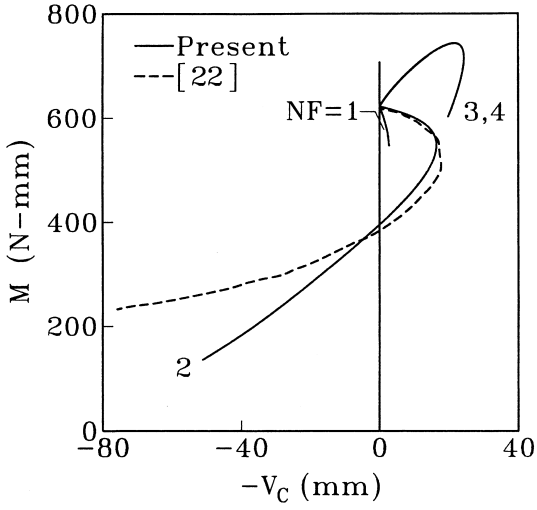

Fig. 16. Load–displacement for simply supported angle subjected to uniform moment.

The results of the present study are obtained by using 48 elements. The buckling load of the present study is 1.0879 N for NF = 1–4. The linear buckling load given by Argyris et al. [5,6] and Hsiao et al. [17] is 1.880 N. Because the prebuckling displacement is negligible, the linear and nonlinear buckling loads are nearly identical. The load–deflection curves are shown in Figs. 11–13. Very good agreement between the results of NF = 2 and the results given in [5,6] is observed. The discrepancy among the results of NF = 1, 2, and 3 is not negligible when the displacements are not small. The results of NF = 3 and 4 are identical. It seems that $(1/2)EK_I \int \mathbf{N}'_d \theta^3_{1,s}\, ds$ is the dominant third-order term.

4.4. Example 4. Simply supported right-angle frame subjected to uniform moment

The example considered here is a simply supported angle frame subjected to uniform moment M as shown in Fig. 14. The ends of the beam are free to rotate about the X_3^G axis, but rotation about X_1^G and

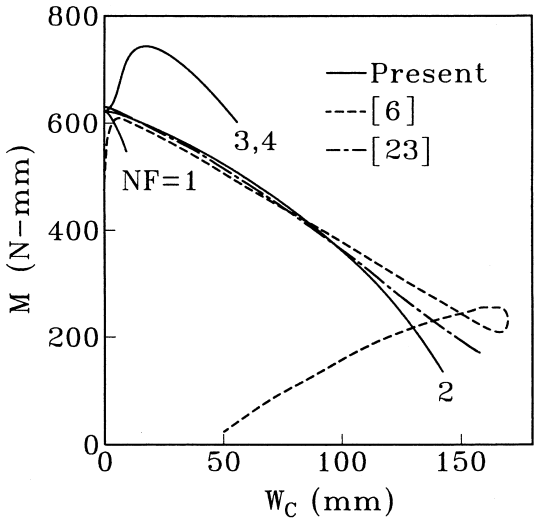

Fig. 17. Load–displacement for simply supported angle subjected to uniform moment.

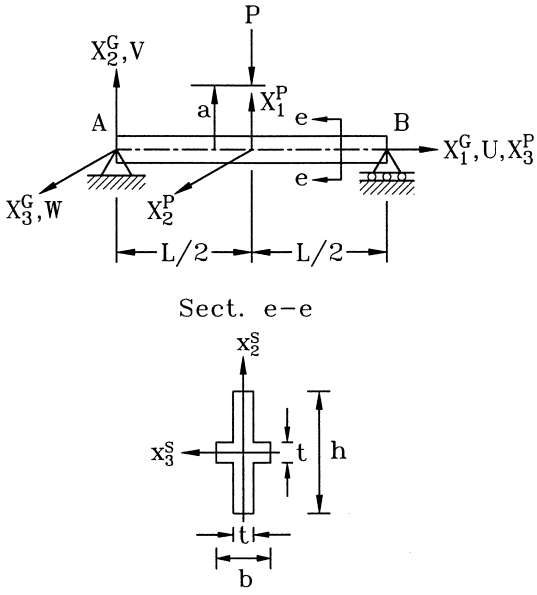

Fig. 18. Simply supported beam subjected to a central concentrated load.

X_2^G axes is prevented. The translation of end point A is restrained, and end point B is free to move in the direction of X_1^G axis. Because of the rotational boundary conditions used here, the ways of generating end moments are rendered irrelevant here. The geometry and material properties are identical with those of Example 3. The theoretical linear buckling moment is $M_{cr} = (\pi/L)\sqrt{EI_y GJ} = 622.21$ N mm [11]. The linear buckling moments given by [3,4,6] and [17] are 624.77 and 624.76 N mm, respectively.

The results of the present study are obtained by using 80 elements. The buckling loads of the present study are 622.37 N mm for NF = 1–4. Because the prebuckling displacement is negligible, the agreement between the linear and nonlinear buckling loads is very good. The load–deflection curves are shown in Figs. 15–17. The agreement between the results of NF = 2 and the results given in [6,22,23] is good when the

Table 1
Buckling loads for simply supported beam with central concentrated load

Load applied at	L (m)	P_{cr} (N)	P_{NB}/P_{cr} [a]
Upper face	1	2460.03	1.014
	2	740.37	1.456
	3	529.85	1.152
	4	354.51	1.105
	5	248.57	1.095
Centroid	1	8382.96	1.130
	2	2095.74	1.130
	3	931.44	1.129
	4	523.94	1.129
	5	335.32	1.129
Lower face	1	19225.96	1.030
	2	3451.12	1.189
	3	1333.03	1.206
	4	693.36	1.200
	5	422.06	1.191

[a] P_{NB} = buckling load of the present study.

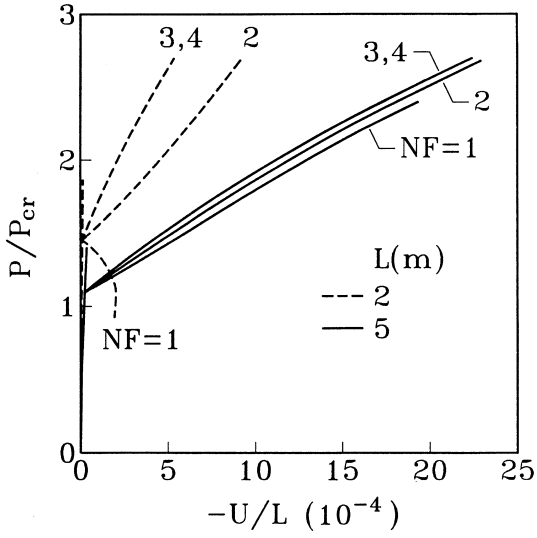

Fig. 19. Load–displacement for simply supported beam (load applied at upper face).

displacements are moderately large. The discrepancy among the results of NF = 1, 2, and 3 is remarked. The results of NF = 3 and 4 are identical. It shows again that $(1/2)EK_I \int \mathbf{N}'_d \theta^3_{1,s}\, ds$ is the dominant third-order term and may not be negligible for very narrow cross sections.

4.5. Example 5. Simply supported beam subjected to a central concentrated load

The example considered here is a simply supported beam subjected to a concentrated load P at the middle as shown in Fig. 18. Here three cases are considered for the application point of P: (1) upper face, (2) centroid, and (3) lower face. The ends of the beam are free to rotate about the X_2^G and X_3^G axes, but rotation about the X_1^G axis is restrained. The translation is restrained at end point A, and is free only in the direction of X_1^G axis at point B. The geometry and material properties are: $L = 1, 2, 3, 4, 5$ m, $b = 0.06$ m,

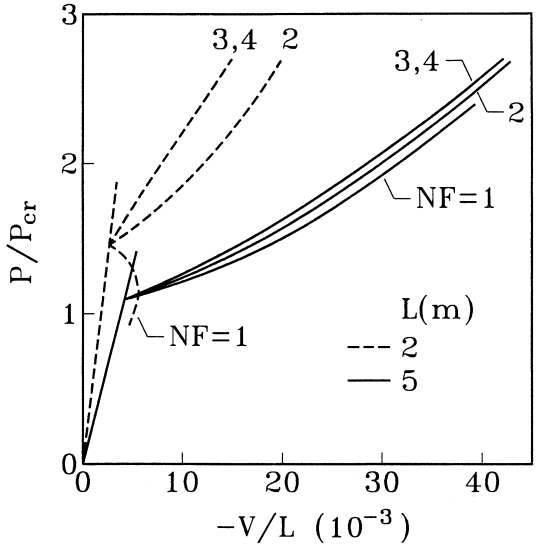

Fig. 20. Load–displacement for simply supported beam (load applied at upper face).

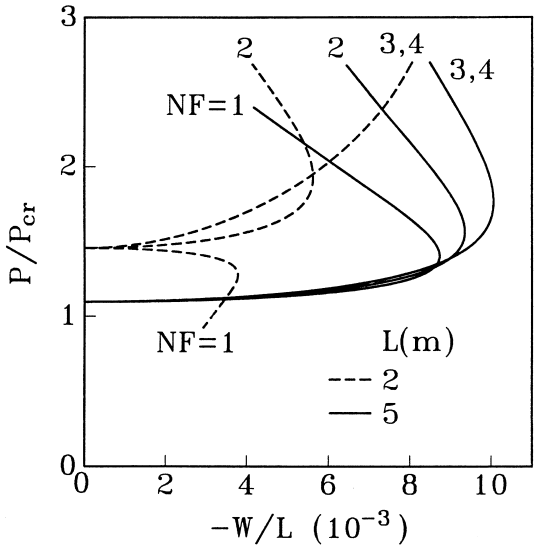

Fig. 21. Load–displacement for simply supported beam (load applied at upper face).

$h = 0.1$ m, $t = 0.002$ m, Young's modulus $E = 2.04 \times 10^{11}$ N/m^2, and shear modulus $G = 7.9 \times 10^{10}$ N/m^2. The classical buckling load is quoted in [11] as

$$P_{\mathrm{cr}} = \frac{16.94\sqrt{EI_y GJ}}{L^2}\left(1 - \frac{1.74a}{L}\sqrt{\frac{EI_y}{GJ}}\right), \quad a = \begin{cases} 0.5h & \text{for upper face,} \\ 0 & \text{for centroid,} \\ -0.5h & \text{for lower face.} \end{cases}$$

The present results are obtained by using 40 elements. The buckling loads for NF = 1–4 are nearly identical. The present buckling loads for NF = 3 are shown in Table 1 together with the linear buckling loads of [11]. As can be seen, when the load is applied at the centroid, the ratios of the present results and

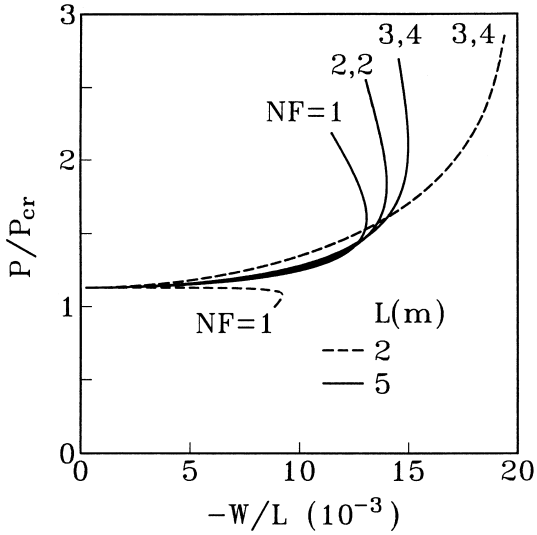

Fig. 22. Load–displacement for simply supported beam (load applied at centroid).

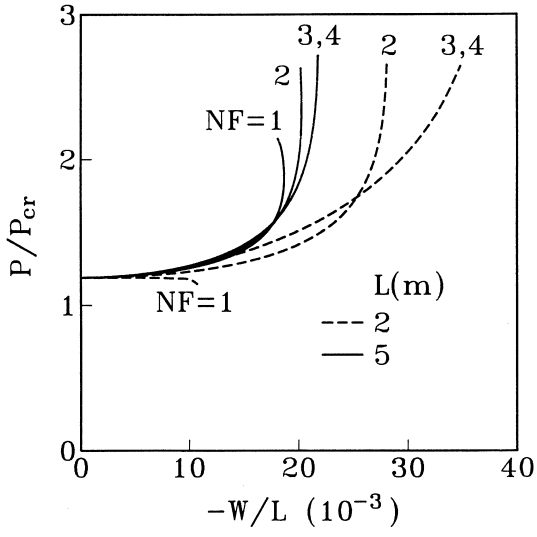

Fig. 23. Load–displacement for simply supported beam (load applied at lower face).

the linear buckling loads are about 1.129 for all lengths of the beam studied. When the load is applied at the upper face, the maximum discrepancy (45.6%) between these two results occurs at $L = 2$ m. The load–deflection curves for different cases are shown in Figs. 19–23. As can be seen the results for NF = 3 and 4 are identical for all cases. The discrepancy among the results for NF = 1, 2, and 3 are remarked especially for the cases of $L = 2$ m. It indicates again that the third-order term $(1/2)EK_I \int \mathbf{N}'_d \theta^3_{1,s}\, ds$ may not be negligible for postbuckling analysis of beams with thin walled open cross section.

4.6. Example 6. Buckling of a cantilever beam subjected to end torsion

The example considered here is a cantilever beam subjected to end torsion T. The quasitangential and semitangential moments are considered. The corresponding load base coordinates are shown in Fig. 24.

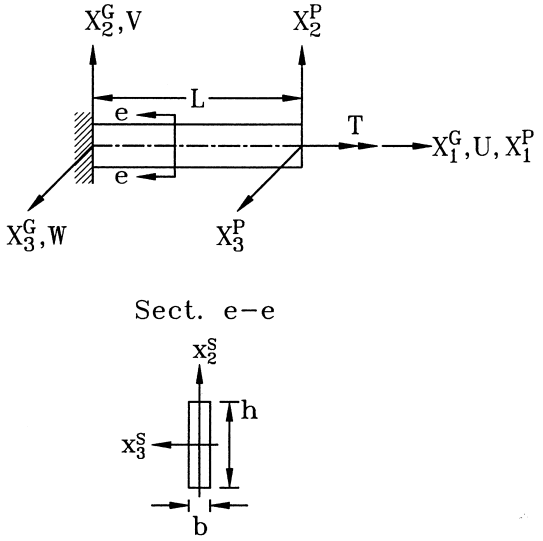

Fig. 24. Cantilever beam subjected to end torsion.

Table 2
Buckling moment for a cantilever beam subjected to end torsion[a]

Type of moment	Number of elements	T_{NB} (10^3 kP cm)			
		NF = 1	NF = 2	NF = 3	NF = 4
QT1	50	2.887	3.213	3.463	3.464
	100	2.921	3.259	3.518	3.519
	150	2.928	3.268	3.529	3.529
	200	2.929	3.271	3.532	3.532
QT2	50	1.450	1.468	1.481	1.481
	100	1.463	1.480	1.494	1.494
	150	1.465	1.483	1.496	1.496
	200	1.466	1.484	1.497	1.497
ST	50	2.605	2.839	3.032	3.032
	100	2.675	2.932	3.146	3.146
	150	2.689	2.951	3.169	3.169
	200	2.694	2.958	3.177	3.178

[a] Classical linear buckling moment [41]

$$T_{cr} = \begin{cases} \frac{\pi E}{2L}\sqrt{I_y I_z} = 1.375 \times 10^4 \text{ kP cm} & \text{for QT,} \\ \frac{\pi E}{L}\sqrt{I_y I_z} = 2.749 \times 10^4 \text{ kP cm} & \text{for ST.} \end{cases}$$

Except $L = 250$ cm, the geometry and material properties are identical with those of Example 1. The classical buckling moment is quoted in [41] as

$$T_{\mathrm{cr}} = \begin{cases} \dfrac{\pi E}{2L}\sqrt{I_y I_z} & \text{for QT,} \\ \dfrac{\pi E}{L}\sqrt{I_y I_z} & \text{for ST.} \end{cases}$$

The present buckling moments are shown in Table 2 together with classical buckling moment [41]. As can be seen, the discrepancy among the buckling moments corresponding to NF = 1–3 is not negligible, and the discrepancy between the present buckling moments and the classical linear buckling moments are remarked. Note that the prebuckling rotations for this example are quite large. The load–deflection curves for different types of moments are shown in Figs. 25–27. As can be seen the results for NF = 3 and 4 are identical for all cases.

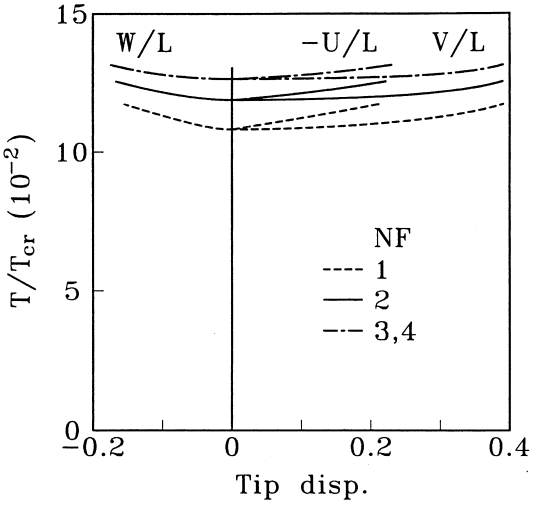

Fig. 25. Load–tip displacement for cantilever beam subjected to end torsion (QT1).

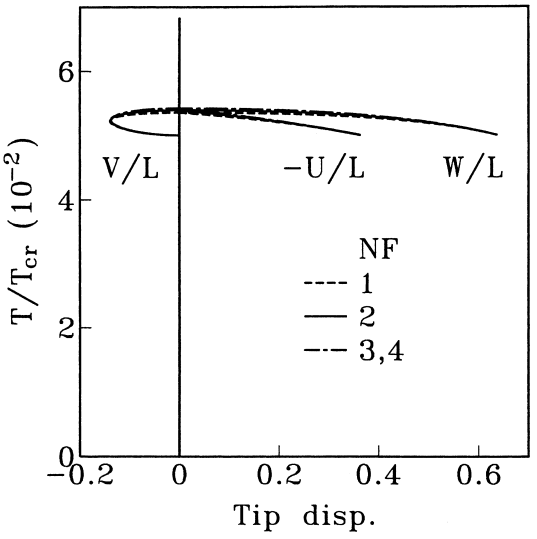

Fig. 26. Load–tip displacements for cantilever beam subjected to end torsion (QT2).

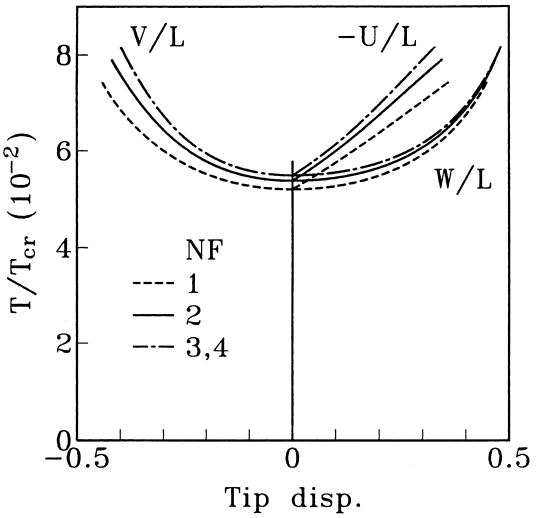

Fig. 27. Load–tip displacements for cantilever beam subjected to end torsion (ST).

5. Conclusions

This paper has proposed a consistent co-rotational finite element formulation and numerical procedure for the buckling and postbuckling analyses of three-dimensional elastic Euler beam. The formulation of beam element proposed in [27] is modified and employed here. All coupling among bending, twisting, and stretching deformations for the beam element is considered by consistent second-order linearization of the fully geometrically nonlinear beam theory. The third-order terms, which are relevant to the twist rate and curvature of the beam axis are also considered. An incremental–iterative method based on the Newton–Raphson method combined with constant arc length of incremental displacement vector is employed for the solution of nonlinear equilibrium equations. The zero value of the tangent stiffness matrix determinant of the structure is used as the criterion of the buckling state. A bisection method of the arc length is proposed to find the buckling load. From the numerical examples studied, it is found that the agreement between the nonlinear buckling loads of the present study and the linear buckling loads given in the literature is very good when the prebuckling displacements are small. However, for cases with large prebuckling displacements, the discrepancy between the nonlinear buckling loads of the present study and the linear buckling loads given in the literature is remarked. Thus when the prebuckling displacements are not negligible, a nonlinear buckling analysis may be required for reliable solutions. The discrepancy among buckling loads for NF = 1–4 is negligible for most examples studied. However, it is observed from the last example that when the prebuckling twist is not small, the effect of third-order terms on the buckling load is not negligible. From the numerical examples studied, it shows that $(1/2)EK_I \int \mathbf{N}'_d \theta^3_{1,s}\,\mathrm{d}s$ is the domainant third-order term. The effect of the third-order term $(1/2)EK_I \int \mathbf{N}'_d \theta^3_{1,s}\,\mathrm{d}s$ may not be negligible for postbuckling analysis of 3-D beams with thin walled open cross section (e.g., rectangular cross section with very small aspect ratio), if the postbuckling behavior is to be determined with accuracy.

References

[1] J.H Argyris, P.C. Dunne, G.A. Malejannakis, E. Schelkle, A simple triangular facet shell element with applications to linear and non-linear equilibrium and elastic stability problems, Comput. Methods Appl. Mech. Engrg. 10 (1977) 371–403.
[2] J.H Argyris, P.C. Dunne, G.A. Malejannakis, E. Schelkle, A simple triangular facet shell element with applications to linear and non-linear equilibrium and elastic stability problems, Comput. Methods Appl. Mech. Engrg. 11 (1977) 97–131.
[3] J.H Argyris, P.C. Dunne, D.W. Scharpf, On large displacement–small strain analysis of structures with rotation degree of freedom, Comput. Methods Appl. Mech. Engrg. 14 (1978) 401–451.
[4] J.H Argyris, P.C. Dunne, D.W. Scharpf, On large displacement–small strain analysis of structures with rotation degree of freedom, Comput. Methods Appl. Mech. Engrg. 15 (1978) 99–135.

[5] J.H. Argyris, O. Hilpert, G.A. Malejannakis, D.W. Scharpf, On the geometrical stiffness of a beam in space – a consistent v.w. approach, Comput. Methods Appl. Mech. Engrg. 20 (1979) 105–131.
[6] J.H. Argyris, H. Balmer, J.St. Doltsinis, P.C. Dunne, M. Haase, M. Kleiber, G.A. Malejannakis, H.P. Mlejenek, M. Muller, D.W. Scharpf, Finite element method – the natural approach, Comput. Methods Appl. Mech. Engrg. 17/18 (1979) 1–106.
[7] J.H. Argyris, S. Symeonidis, Nonlinear finite element analysis of elastic systems under nonconservative loading-natural formulation. Part I: quasistatic problems, Comput. Methods Appl. Mech. Engrg. 26 (1981) 75–123.
[8] D.O. Brush, B.O. Almroth, Buckling of Bars, Plates and Shells, McGraw-Hill, New York, 1975.
[9] W.F. Chen, E.M. Lui, Structural Stability, Theory and Implementation, Elsevier, New York, 1988.
[10] V.Z. Vlasov, Thin Walled Elastic Beams, second ed., (English translation published for US Science Foundation by Israel Program for Scientific Translations), 1961.
[11] S.P. Timoshenko, J.M. Gere, Theory of Elastic Stability, second ed., McGraw-Hill, New York, 1963.
[12] R.S. Barsoum, R.H. Gallagher, Finite element analysis of torsional and torsional-flexural stability problems, moments, Internat. J. Numer. Methods Engrg. 2 (1970) 335–352.
[13] H. Ziegler, Principles of Structural Stability, Birkhauser, Basel, 1977.
[14] M.M. Attard, Lateral buckling analysis of beams by FEM, Comput. Struct. 23 (1986) 217–231.
[15] A.F. Saleeb, T.Y.P. Chang, A.S. Gendy, Effective modeling of spatial buckling of beam assemblages, accounting for warping constraints and rotation-dependency of moments, Internat. J. Numer. Methods Engrg. 33 (1992) 469–502.
[16] M.Y. Kim, S.P. Chang, S.B. Kim, Spatial stability analysis of thin walled space frames, Internat. J. Numer. Methods Engrg. 39 (1996) 499–525.
[17] K.M. Hsiao, R.T. Yang, W.Y. Lin, A consistent finite element formulation for linear buckling analysis of spatial beams, Comput. Methods Appl. Mech. Engrg. 156 (1998) 259–276.
[18] J.C. Simo, L. Vu-Quoc, A three-dimensional finite strain rod model. Part II: computational aspects, Comput. Methods Appl. Mech. Engrg. 58 (1986) 79–116.
[19] M.A. Crisfield, A consistent co-rotational formulation for non-linear, three-dimensional, beam elements, Comput. Methods Appl. Mech. Engrg. 81 (1990) 131–150.
[20] A.S. Gendy, A.F. Saleeb, Generalized mixed finite element model for pre-and post-quasistatic buckling response of thin-walled framed structures, Internat. J. Numer. Meths. Engrg. 37 (1994) 297–322.
[21] H. Lee, D.W. Jung, J.H. Jeong, S. Im, Finite element analysis of lateral buckling for beam structures, Comput. Struct. 53 (1994) 1357–1371.
[22] G. Jelenic, M. Saje, A kinematically exact space finite strain beam model-finite element formulation by generalized virtual work principle, Comput. Methods Appl. Mech. Engrg. 120 (1995) 131–161.
[23] A. Ibrahimbegovic, H. Shakourzadeh, J.L. Batoz, M.A. Mikdad, Y.Q. Gao, On the role of geometrically exact and second-order theories in buckling and post-buckling analysis of three-dimensional beam structures, Comput. Struct. 61 (1996) 1101–1114.
[24] Y. Goto, X.S. Li, T. Kasugal, Buckling analysis of elastic space rods under torsional moment, J. Engrg. Mech. ASCE 122 (1996) 826–833.
[25] A. Cardona, M. Geradin, A beam finite element non-linear theory with finite rotations, Internat. J. Numer. Methods Engrg. 26 (1988) 2403–2438.
[26] M. Iura, S.N. Atluri, On a consistent theory and variational formulation of finitely stretched and rotated 3-D spaced-curved beams, Comput. Mech. 4 (1989) 73–88.
[27] K.M. Hsiao, Corotational total Lagrangian formulation for three-dimensional beam element, AIAA J. 30 (1992) 797–804.
[28] K. Mattiasson, A. Samuelsson, Total and updated Lagrangian forms of the co-rotational finite element formulation in geometrically and materially nonlinear analysis, in: C. Tailor, E. Hinton, D.R.J. Owen (Eds.), Numerical Methods for Non-linear Problems, vol. 2, Pineridge Press, Swansea, UK, 1984, pp. 135–151.
[29] J.C. Simo, L. Vu-Quoc, The role of non-linear theories in transient dynamic analysis of flexible structures, J. Sound Vibration 119 (1987) 487–508.
[30] K.M. Hsiao, W.I. Lin, A second order beam theory, in: Proceedings of the Fourth World Congress on Computational Mechanics, Buenos Aires, Argentina, 1998.
[31] T. Matsui, O. Matsuoka, A new finite element scheme for instability analysis of thin shells, Internat. J. Numer. Methods Engrg. 10 (1976) 145–170.
[32] H. Goldstein, Classical Mechanics, Addision-Wesley, Reading, MA, 1980.
[33] D.J. Dawe, Matrix and Finite Element Displacement Analysis of Structures, Oxford University Press, New York, 1984.
[34] T.J. Chung, Continuum Mechanics, Prentice-Hall, Englewood Cliffs, NJ, 1988.
[35] K.S. Schweizerhof, E. Ramm, Displacement dependent pressure loads in nonlinear finite element analysis, Comput. Struct. 18 (1984) 1099–1114.
[36] K.J. Bathe, Finite Element Procedure in Engineering Analysis, Prentice-Hall, Englewood Cliffs, NJ, 1982.
[37] M.A. Crisfield, A fast incremental/iterative solution procedure that handles snap through, Comput. Struct. 13 (1981) 55–62.
[38] K.M. Hsiao, H.J. Horng, Y.R. Chen, A corotational procedure that handles large rotations of spatial beam structures, Comput. Struct. 27 (1987) 769–781.
[39] K.M. Hsiao, C.M. Tsay, A motion process for large displacement analysis of spatial frames, Internat. J. Space Struct. 6 (1991) 133–139.
[40] K.M. Hsiao, Nonlinear analysis of general shell structures by flat triangular shell element, Comput. Struct. 25 (1987) 665–675.
[41] Y.B. Yang, S.R. Kuo, Buckling of frames under various torsional loading, J. Engrg. Mech. ASCE 117 (1991) 1681–1697.